doi:10.1093/mnras/sty2786

Downloaded from https://academic.oup.com/mnras/article-abstract/482/2/2132/5132880 by University of Wisconsin-Madison Libraries user on 21 June 2019



Siva Darbha, ^{1★} Eric R. Coughlin ⁶, ^{2,3}† Daniel Kasen ^{1,2,4} and Eliot Quataert ^{1,2}

Accepted 2018 October 12. Received 2018 October 11; in original form 2018 June 14

ABSTRACT

Supermassive black holes (SMBHs) in galactic nuclei can eject hypervelocity stars (HVSs). Using restricted three-body integrations, we study the properties of stars ejected by circular, binary SMBHs as a function of their mass ratios $q=M_2/M_1$ and separations a, focusing on the stellar velocity and angular distributions. We find that the ejection probability is an increasing function of q and a, and that the mean ejected velocity scales with q and a similar to previous work but with modified scaling constants. Binary SMBHs tend to eject their fastest stars towards the binary orbital plane. We calculate the ejection rates as the binary SMBHs inspiral, and find that they eject stars with velocities $v_{\infty} > 1000 \, \mathrm{km \, s^{-1}}$ at rates of $\sim 4 \times 10^{-2}$ $-2 \times 10^{-1} \, \mathrm{yr^{-1}}$ for $q=1 \, (\sim 10^{-4} - 10^{-3} \, \mathrm{yr^{-1}}$ for q=0.01) over their lifetimes, and can emit a burst of HVSs with $v_{\infty} > 3000 \, \mathrm{km \, s^{-1}}$ as they coalesce. We integrate the stellar distributions over the binary SMBH inspiral and compare them to those produced by the 'Hills mechanism' (in which a single SMBH ejects a star after tidally separating a binary star system), and find that $N \sim 100 \, \mathrm{HVS}$ velocity samples with $v_{\infty} \gtrsim 200 \, \mathrm{km \, s^{-1}}$ are needed to confidently distinguish between a binary and single SMBH origin.

Key words: black hole physics – stars: kinematics and dynamics – stars: statistics – galaxies: nuclei.

1 INTRODUCTION

Supermassive black holes (SMBHs) in the centres of galaxies can eject stars with velocities $\tilde{v} \gtrsim 1000~\rm km\,s^{-1}$ (Hills 1988; Yu & Tremaine 2003; Brown 2015). These hypervelocity stars (HVSs) can be used to probe galactic BHs and their stellar environments. In particular, the properties of HVSs can reveal the presence of a single or binary SMBH in a galaxy's core (Yu & Tremaine 2003), illuminate a galaxy's star formation history (Kollmeier & Gould 2007), and constrain the shape of a galactic potential generated by both ordinary and dark matter (Gnedin et al. 2005; Kenyon et al. 2014; Rossi et al. 2017; Fragione & Loeb 2017).

Several hypervelocity stars have been observed in the Milky Way (Brown et al. 2005, 2015), and the high-precision data from the Global Astrometric Interferometer for Astrophysics (GAIA) (Kenyon et al. 2014; Boubert et al. 2018; Brown et al. 2018; Marchetti, Rossi & Brown 2018a; Marchetti et al. 2018b) and the Large Synoptic Survey Telescope (LSST) (LSST Science Collaboration et al. 2009) will likely produce a catalogue of thousands

* E-mail: siva.darbha@berkeley.edu † Einstein fellow. more. Indeed, HVSs are currently detectable only near the Milky Way (a constraint that will continue into the near future), and those observed will likely originate from the Galactic Centre (GC) (Brown 2015). A subset may also arise from satellite galaxies, particularly the Large Magellanic Cloud (LMC) (Edelmann et al. 2005; Gualandris & Portegies Zwart 2007; Boubert & Evans 2016; Erkal et al. 2018), and a small number may come from the Andromeda galaxy (M31) (Sherwin, Loeb & O'Leary 2008).

SMBHs can expel HVSs by three general classes of encounters: (1) a stellar binary encounters a single SMBH as a 'slow intruder' (i.e. the velocity of the binary centre-of-mass at infinity relative to the SMBH is lower than the binary orbital velocity; Hills 1989), the black hole replaces one of the stars in an exchange collision, and the dislodged star departs with a high velocity (the 'Hills mechanism,' Hills 1988); (2) a single star encounters a binary SMBH as a 'slow intruder,' and is ejected with an enhanced velocity after extracting some of the binary SMBH energy (Yu & Tremaine 2003); and (3) a star is bound to one SMBH and is ejected after an encounter with the second SMBH (Gualandris, Portegies Zwart & Sipior 2005; Guillochon & Loeb 2015). The rates of ejection and the properties of HVSs differ depending on the means of production.

Although HVSs can be produced by other means, including a supernova explosion by one constituent of a compact binary (Blaauw

¹Department of Physics, University of California, Berkeley, Berkeley, CA 94720, USA

²Department of Astronomy and Theoretical Astrophysics Center, University of California, Berkeley, Berkeley, CA 94720, USA

³Columbia Astrophysics Laboratory, Columbia University, New York, NY 10027, USA

⁴Nuclear Science Division, Lawrence Berkeley National Laboratory, Berkeley, CA 94720, USA

1961), close encounters between single stars (Yu & Tremaine 2003), close encounters between star clusters and central SMBHs (Arca Sedda et al. 2017; Fragione et al. 2017), and scattering between stars and stellar mass black hole clusters in the potential of an SMBH (Miralda-Escudé & Gould 2000; O'Leary & Loeb 2008), most are expected to have SMBH origins (Yu & Tremaine 2003; Gualandris et al. 2005; Brown 2015), and thus the production channels listed above have been investigated in detail. Hypervelocity stars produced by the Hills mechanism have been studied extensively (e.g. Hills 1988; Yu & Tremaine 2003; Bromley et al. 2006; Kenyon et al. 2008; Rossi, Kobayashi & Sari 2014; Brown 2015). An SMBH binary origin for HVSs (henceforth labelled the 'SMBHB mechanism,' including both 2 and 3 above) has also received attention (Quinlan 1996; Zier & Biermann 2001; Yu & Tremaine 2003), both when the binary ejects incident unbound stars (Yu & Tremaine 2003; Sesana, Haardt & Madau 2006, 2007b) or bound stars (Sesana, Haardt & Madau 2008), the latter most often when an IMBH inspirals towards an SMBH (Gualandris et al. 2005; Baumgardt, Gualandris & Portegies Zwart 2006; Levin 2006; Sesana, Haardt & Madau 2007a; Löckmann & Baumgardt 2008; Sesana et al. 2008).

Several features of the velocity distribution of HVSs have been illuminated that can be used to distinguish these two mechanisms. For example, the SMBHB mechanism can eject stars at a rate upwards of ~ 10 times higher than the Hills mechanism. The average ejection velocity of the Hills mechanism depends on the mass of the stellar binary, whereas that of the SMBHB mechanism is agnostic to the stellar properties (Hills 1988; Yu & Tremaine 2003). SMBH binaries can produce velocity distributions with more variable extrema owing to the additional channels and degrees of freedom available in their interactions with stars (Gualandris et al. 2005; Baumgardt et al. 2006; Sesana et al. 2006, 2007a). HVSs (all those with $\tilde{v} \gtrsim 1000 \, \mathrm{km \, s^{-1}}$) produced by the Hills mechanism are ejected isotropically, whereas those from the SMBHB mechanism have a more complicated angular behaviour: for circular SMBH binaries, HVSs are preferentially ejected in the binary orbital plane for nearly equal-mass ratios and wider binaries, but more isotropically for lower mass ratios and tighter binaries (Zier & Biermann 2001; Baumgardt et al. 2006; Levin 2006; Sesana et al. 2006). The Hills mechanism will eject HVSs as long as there is a continuous supply of stellar binaries, whereas the SMBHB mechanism ejects a burst of HVSs in $t \sim 1 - 10$ Myr; this occurs when both a contracting binary SMBH ejects incident unbound stars (Sesana et al. 2006, 2007b) or inspirals through a stellar cusp (Baumgardt et al. 2006; Levin 2006; Sesana et al. 2008).

In order to determine the specific mechanism that produces observed HVSs arising from different galaxies, and thus infer the existence or binarity of SMBHs in a given galactic nucleus, one must undertake a systematic study of the properties of HVSs produced by binary SMBHs, and compare them to those produced by the Hills mechanism under realistic conditions. At present, this comparison can help to distinguish between the presence of a single or binary SMBH in the Milky Way, one of its satellite galaxies, or even Andromeda. As astrometry improves, this analysis can be extended to other nearby galaxies.

This paper is the second in a two-part sequence. In the first part, we investigated the statistics of tidal disruption events (TDEs) by binary SMBHs over a range of binary mass ratios and separations (Darbha et al. 2018), ¹ extending the work of Coughlin et al. (2017)

(also see Coughlin & Armitage 2018 for an application to an observed event). In this paper, we study the hypervelocity stars ejected by these SMBH binaries over the same parameter range. The set-up and inputs of our simulations partly overlap with those of previous studies, though we focus more exclusively on circular, nearly equalmass SMBH binaries and have a more densely populated parameter space in mass ratio and separation, so our results can corroborate earlier work and have the potential to reveal new features.

In Section 2, we briefly recapitulate our simulation set-up; a more detailed overview can be found in Darbha et al. (2018). In Section 3, we present the ejection probability and the properties of the ejected stars, namely their velocity and angular distributions. We then present the time-dependent ejection rate as the SMBH binary contracts due to stellar scattering and gravitational wave emission. In Section 4, we compare the integrated distributions for stars ejected by a binary and single SMBH, a more realistic treatment than previously considered in this parameter regime. To conclude, we present the number samples needed to distinguish between the SMBHB and Hills mechanisms, and to identify the progenitor's properties. We summarize our results in Section 5.

2 SIMULATION SET-UP

We study the properties of hypervelocity stars ejected by 'hard' SMBH binaries when the stars are initially incident from the loss cone in the 'pinhole' (or 'full loss cone') regime (Frank & Rees 1976; Lightman & Shapiro 1977; Cohn & Kulsrud 1978; Magorrian & Tremaine 1999). A binary SMBH becomes 'hard' at roughly the separation (Quinlan 1996)

$$\tilde{a}_{\rm h} = \frac{GM_1M_2}{4(M_1 + M_2)\sigma^2},\tag{1}$$

where M_1 and M_2 are the masses of the primary and secondary, and σ is the 1D velocity dispersion of the stars in the galactic nucleus. We discussed our assumption of 'hard' binaries and the 'full loss cone' regime in the first part of this two-paper sequence (Darbha et al. 2018), and direct the reader there for a more detailed discussion.

Stars incident from the loss cone can be ejected only if they are not first tidally disrupted. A star that approaches an SMBH too closely gets tidally disrupted when the tidal gravity from the SMBH overwhelms the self-gravity of the star. Disruption occurs at the tidal radius, which is roughly equal to $\tilde{r}_t \simeq R_* (M_{\bullet}/M_*)^{1/3}$, where M_{\bullet} is the black hole mass and M_* and R_* are the star's mass and radius. We adopt this definition of the tidal radius and assume that all stars that enter it are completely disrupted, ignoring complications owing to stellar structure (Lodato, King & Pringle 2009; Guillochon & Ramirez-Ruiz 2013; Mainetti et al. 2017).

We outlined our set-up and described its domain of validity in our first paper (Darbha et al. 2018). To briefly summarize, we use Mathematica to simulate stars incident on a binary SMBH in the circular restricted three-body approximation, in the point particle limit, and using Newtonian gravitational potentials. We write our simulation parameters in the units $G = M = \tilde{a} = 1$, where $M = M_1 + M_2$ is the total binary SMBH mass and \tilde{a} is its separation. The SMBH binary is then described by two dimensionless quantities: the mass ratio $q = M_2/M_1$ and the primary's (dimensionless) tidal

caption describing them in Figure 12. The notation and terminology were also unclear at times. We have corrected similar work in this paper, which can be used for reference.

¹There were a few minor mistakes in the published version of the first paper. There was a mistake in the error bars in Figures 7, 12, and 14, and in the

2134 S. Darbha et al.

Table 1. The quantities used to non-dimensionalize variables (with the dimensions length, mass, time, velocity, and stellar specific energy) in different sections of the paper, unless stated otherwise. Throughout the paper, if the dimensional character of a variable is not clear from the context, then we write dimensioned variables with tildes on top and dimensionless ones without them. The parentheses show the definitions of some variables used in each section.

Section	Length	Mass	Time	Velocity	Specific energy (ϵ)
Simulation (2)	ã	$M = M_1 + M_2$	$\sqrt{\tilde{a}^3/GM}$	$v_{\rm bin} = \sqrt{GM/\tilde{a}}$	GM/\tilde{a}
Ejection probability (3.1)	$ \begin{aligned} \tilde{r}_{t1} \\ (a = \tilde{a}/\tilde{r}_{t1}) \end{aligned} $				
Ejection properties (3.2)	$ \tilde{r}_{t1} $ $ (a = \tilde{a}/\tilde{r}_{t1}) $	M_1		$v_0 = \sqrt{GM_1/\tilde{r}_{t1}}$ $(v = \tilde{v}/v_0)$	
Ejection rate (3.3)	$ \tilde{r}_{t1} \\ (a = \tilde{a}/\tilde{r}_{t1}) $	M_1	$t_0 = \tilde{r}_{t1}^4 c^5 / G^3 M_1^3$ $(t = \tilde{t}/t_0)$	(* -7-07	$GM_1/\tilde{r}_{ m t1}$
Comparison (4): Binary SMBH	$ \tilde{r}_{t1} \\ (a = \tilde{a}/\tilde{r}_{t1}) $		(, , ,	$v_{\rm bin} = \sqrt{GM/\tilde{a}}$ $(v = \tilde{v}/v_{\rm bin})$	
Comparison (4): Binary star	$a_{*0} = 1$ au $(a_* = \tilde{a}_*/a_{*0})$			$v_* = \sqrt{Gm_{\text{tot}}/\tilde{a}_*}$ $(v = \tilde{v}/v_*)$	

radius $r_{t1} = \tilde{r}_{t1}/\tilde{a}$. We set the origin of the coordinate system to the binary SMBH centre of mass. The stars begin on parabolic (specific energy $\epsilon = 0$) orbits with respect to the origin, and are distributed isotropically over a sphere of radius r = 50. The specific angular momentum ℓ of each star is sampled such that its square is uniformly distributed in the range $\ell^2 \in [0, 4]$ (yielding uniformly distributed pericentres $r_p \in [0, 2]$), which corresponds to the 'pinhole' (or 'full loss cone') regime. An integration terminates if the star crosses the tidal radius of one of the BHs, if it escapes to r = 100, or if the simulation time reaches $t = 10^4$. A large fraction of the 'escaped' stars have positive energy and will thus be 'ejected' from the binary SMBH; we use this terminology throughout to distinguish between these two outcomes. We explore many points in the parameter range $q \in [0.01, 1]$ and $r_{t1} \in [0.001, 0.1]$ ($\tilde{a}/\tilde{r}_{t1} \in [10, 1000]$), and simulate 5×10^6 encounters for each point. For comparison, we simulated a smaller number of encounters for a few points in our parameter space with the N-body code REBOUND using the IAS15 integrator (Rein & Liu 2012; Rein & Spiegel 2015), and found close agreement with our results.

Though we vary these two binary SMBH quantities in our simulations, we ultimately interpret these in our results as varying \tilde{a} and M_2 while holding \tilde{r}_{t1} and M_1 fixed. Note that we do not hold the total mass M fixed, in contrast to other studies. In this paper, if the dimensional character of a variable is not clear from the context, then we write dimensioned variables with tildes on top and dimensionless ones without them. Table 1 presents the different scales we use to define dimensionless variables in different sections of the paper, unless otherwise noted.

We take as our main example a primary with mass $M_1=10^6\,\mathrm{M}_\odot$ and stars with solar parameters. The primary's tidal radius is then $\tilde{r}_{t1}=2.3\,\mu\mathrm{pc}$ and the range of separations is $\tilde{a}\in[0.023,2.3]$ mpc. The characteristic orbital velocity of a binary SMBH is $v_\mathrm{bin}=\sqrt{GM/\tilde{a}}\sim2000\,\mathrm{km\,s^{-1}}$ for $M\sim10^6\,\mathrm{M}_\odot$ and $\tilde{a}\sim10^{-3}\,\mathrm{pc}$, and the velocities of the stars in the bulge are $\sigma\sim100\,\mathrm{km\,s^{-1}}$ for a Milky Way-like galaxy (Gültekin et al. 2009). Since $\sigma\ll v_\mathrm{bin}$, the stars are 'slow intruders' (Hills 1989) and will be expelled with enhanced velocities in most encounters with the SMBH binary.

For comparison, Quinlan (1996) and Sesana et al. (2006) studied incident unbound stars on mildly hyperbolic orbits. They set up their stars with initial velocities $\tilde{v}_i \ll v_{\rm bin}$; in this regime, scattering is not sensitive to the initial velocity (Quinlan 1996), so their mildly hyperbolic orbits and our parabolic orbits should behave similarly. The above Authors also initialized the stars with a uniform distribution in b^2 , where b is the impact parameter, and with pericenters

 $\tilde{r}_p \leq \text{few} \times \tilde{a}$. Since $\tilde{v}_i \ll v_{\text{bin}}$ and $\tilde{r}_p \sim \tilde{a}$, the uniform distribution in b^2 implies a roughly uniform distribution in r_p as well, as in this work. However, they adopted stricter criteria to classify an event as an 'ejection' than we do (Section 3); in particular, they imposed an additional velocity cutoff to incorporate the bulge gravity.

3 HYPERVELOCITY STARS

In this section, we study in detail the influence of the binary mass ratio and separation on the stellar ejections. We examine the ejection probability (Section 3.1) and the properties of the ejected stars (Section 3.2), in particular their distributions in velocity and direction

Throughout this paper, we use the following terminology to distinguish between two possible end states for expelled stars. We label a star as 'escaped' if it reaches $r_{100} = \tilde{r}_{100}/\tilde{a} \equiv 100$ and terminate the integration, as these stars have effectively left the binary SMBH sphere of influence in most galaxies. We label a star as 'ejected' if it escapes with positive specific energy $\epsilon = \tilde{\epsilon}/(GM/\tilde{a}) > 0$, and will thus reach $r = \tilde{r}/\tilde{a} \to \infty$ if the binary SMBH is the only source of gravity. In a multipole expansion of the binary SMBH potential (written in its centre-of-mass frame and evaluated at a field point at r_{100}), the dipole term vanishes and the ratio of the quadrupole to monopole terms is $\Phi_{\ell=2}/\Phi_{\ell=0} \sim (1/r_{100})^2 = 10^{-4}$. The monopole term thus dominates, so the specific energy ϵ_{100} of the ejected stars at r_{100} will be roughly conserved, and their velocities will be $v_{\infty} = \tilde{v}_{\infty}/v_{\rm bin} \simeq \sqrt{2\epsilon_{100}}$ as $r \to \infty$.

3.1 Ejection probability

Fig. 1 shows the escape probability $\lambda_{\rm esc} = N_{\rm esc}/N_{\rm e}$, where $N_{\rm esc}$ ($N_{\rm e} = 5 \times 10^6$) is the number of escapes (encounters). Stars escape the simulation in most encounters (≥ 86 per cent), and are disrupted (≤ 12 per cent) or time-out (≤ 2 per cent) for the rest. The escape probability is largely independent of $q = M_2/M_1$ for $q \gtrsim 0.2$, and for a given q, it decreases as the binary SMBH contracts. At large separations, equal-mass SMBH binaries cause more stars to escape, and at small separations the opposite trend holds, with a transition at $a = \tilde{a}/\tilde{r}_{t1} \simeq 100$, where $\lambda_{\rm esc}$ is roughly independent of q over the entire range we explored.

Fig. 2 shows the ejection probability $\lambda_{\rm ej} = N_{\rm ej}/N_{\rm e}$ for the SMBHB mechanism, where $N_{\rm ej}$ ($N_{\rm e} = 5 \times 10^6$) is the number of ejections (encounters). The probability is a monotonically increasing function of both a and q, and is roughly independent of a for $a \gtrsim 100$ and of

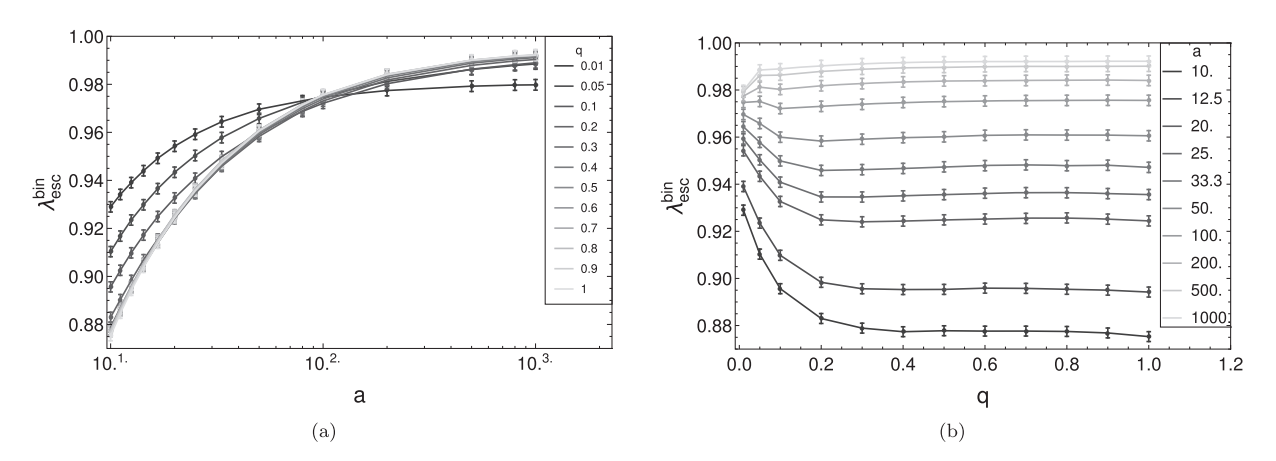


Figure 1. The escape probability $\lambda_{\rm esc} = N_{\rm esc}/N_{\rm e}$ for the SMBHB mechanism, plotted versus (a) $a = \tilde{a}/\tilde{r}_{t1}$ and (b) $q = M_2/M_1$, where $N_{\rm esc}$ ($N_{\rm e} = 5 \times 10^6$) is the number of escapes (encounters), and where an 'escape' occurs when a star crosses the sphere at $\tilde{r}/\tilde{a} = 100$. The error bars have half-widths 5σ , where $\sigma = (\lambda_{\rm esc}/N_{\rm e})^{1/2}$ are the standard errors assuming a Poisson distribution.

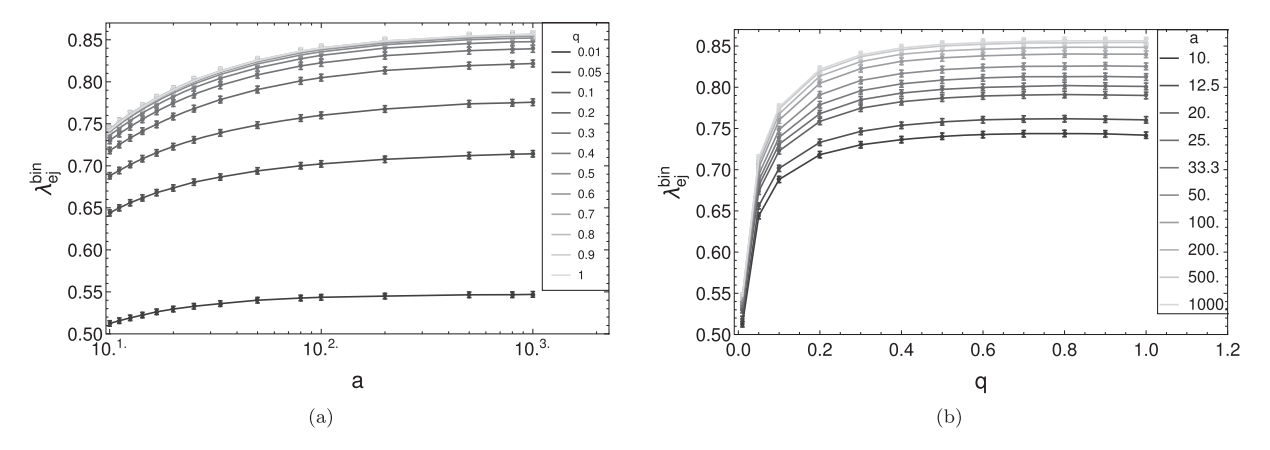


Figure 2. The ejection probability $\lambda_{\rm ej} = N_{\rm ej}/N_{\rm e}$ for the SMBHB mechanism, plotted versus (a) $a = \tilde{a}/\tilde{r}_{t1}$ and (b) $q = M_2/M_1$, where $N_{\rm ej}$ ($N_{\rm e} = 5 \times 10^6$) is the number of ejections (encounters), and where an 'ejection' occurs when a star crosses the sphere at $\tilde{r}/\tilde{a} = 100$ with positive energy. The error bars have half-widths 10σ , where $\sigma = (\lambda_{\rm ej}/N_{\rm e})^{1/2}$ are the standard errors assuming a Poisson distribution.

q for $q \gtrsim 0.2$. The probability is lower than the escape probability, since a subset of stars that cross the escape sphere are on very weakly bound elliptical orbits. This reduction is more pronounced for lower mass ratios, since a lower mass secondary tends to only lightly perturb the incident stars, shifting them from an initial parabolic orbit to a highly elliptical one.

The mass ejection rates found by Quinlan (1996) and Sesana et al. (2006) for circular SMBH binaries exhibit a different trend from the ejection probabilities that we find here. Their rates decrease with increasing \tilde{a}/\tilde{a}_h and their curves for different q crossover. This difference is likely due to the stricter definition of an 'ejection' that they adopt while studying the hardening of the binary, as mentioned before. We incorporate cutoffs for the velocities tof the ejected stars in Section 3.2, and find a similar dependence as the above Authors.

3.2 Properties of ejected stars

We now turn to the properties of the ejected hypervelocity stars, namely their velocity (Section 3.2.1) and angular (Section 3.2.2) distributions. We rewrite our variables in the units $G = M_1 = \tilde{r}_{t1} = 1$, since these quantities are fixed for different SMBH binary mass ratios and separations. In particular, the velocities are normalized

using the scale

$$v_0 = \sqrt{\frac{GM_1}{\tilde{r}_{t1}}}$$

$$\simeq 4.4 \times 10^4 \,\mathrm{km \, s^{-1}} \left(\frac{M_1}{10^6 \,\mathrm{M}_\odot}\right)^{1/3} \left(\frac{M_*}{1 \,\mathrm{M}_\odot}\right)^{1/6} \left(\frac{R_*}{1 \,\mathrm{R}_\odot}\right)^{-1/2}.$$
(2)

The characteristic circular velocity of a binary SMBH of total mass M and semi-major axis \tilde{a} is then simply $v_{\rm bh} = \sqrt{GM/\tilde{a}} = v_0\sqrt{(1+q)/a}$, where $a = \tilde{a}/\tilde{r}_{\rm tl}$, or dimensionally

$$v_{\rm bh} \simeq 2070 \,\mathrm{km} \,\mathrm{s}^{-1} \left(\frac{M}{10^6 \,\mathrm{M}_\odot}\right)^{1/2} \left(\frac{\tilde{a}}{1 \,\mathrm{mpc}}\right)^{-1/2}.$$
 (3)

Where necessary, we consider as our central example a primary with mass $M_1=10^6\,{\rm M}_\odot$ and stars with solar parameters, yielding $v_0\simeq 4.4\times 10^4\,{\rm km\,s^{-1}}$.

3.2.1 Velocity distribution

Fig. 3 shows the mean velocity $\langle \tilde{v}_\infty \rangle$ of the ejected stars. The curves show the data points fit to the function (based on the work of Yu &

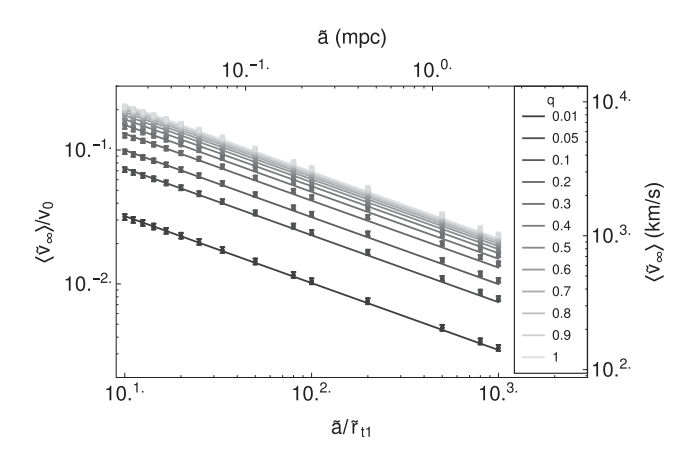


Figure 3. The mean velocity $\langle \tilde{v}_{\infty} \rangle$ of the ejected stars as a function of the binary SMBH separation \tilde{a} and for several mass ratios $q = M_2/M_1$. The error bars have half-widths $100\sigma_{\rm e}$, where $\sigma_{\rm e} = \sigma/\sqrt{N_{\rm ej}}$ is the standard error in the mean and σ is the standard deviation. The curves that fit the data are given by equation (4). The dimensioned axes were calculated for $M_1 = 10^6 \, {\rm M}_{\odot}$ and stars with solar parameters.

Tremaine 2003, discussed below)

$$\langle \tilde{v}_{\infty} \rangle \simeq \kappa v_0 \left(\frac{q}{1+q} \right)^{1/2} \left(\frac{\tilde{a}}{\tilde{r}_{\rm tl}} \right)^{-1/2},$$
 (4)

where κ is a q-dependent dimensionless parameter. The parameter is in the range $0.97 \le \kappa \le 1.06$, and we find that it is well described by $\kappa \simeq \alpha \mathrm{e}^{-\beta q} + \gamma$ for $q \gtrsim 0.05$, where $\alpha \simeq 0.10$, $\beta \simeq 2.5$, and $\gamma \simeq 0.96$. It decreases for lower q, as we find $\kappa \simeq 1.02$ for q = 0.01. The mean is thus set by the velocity of the reduced mass $\mu = M_1 M_2 I (M_1 + M_2)$ of the circular SMBH binary, $\langle \tilde{v}_{\infty} \rangle \sim (G \mu / \tilde{a})^{1/2}$, since an incident star effectively encounters this on average; the parameter κ describes the mean deviation from this, which is on the order of a few per cent.

Yu & Tremaine (2003) approximate the mean velocity as $\langle \tilde{v}_{\infty} \rangle \simeq \sqrt{2 \langle \tilde{\epsilon}_{\infty} \rangle}$, where they express the mean specific energy of the ejected stars as $\langle \tilde{\epsilon}_{\infty} \rangle \simeq KG\mu/\tilde{a}$ for a dimensionless constant K that parametrizes the energy the stars extract from the binary SMBH (Yu 2002). Yu & Tremaine (2003) find a constant $\kappa \simeq \sqrt{3.2} \simeq 1.79$ (from $K \simeq 1.6$) using the typical hardening rate $H \simeq 16$ found by Quinlan (1996). If we use this definition of $\langle \tilde{v}_{\infty} \rangle$ instead and fit our data to equation (4), then we find $1.19 \le \kappa \le 1.33$, lower than that used by Yu & Tremaine (2003), and the same fitting curve for $q \gtrsim 0.05$ with $\alpha \simeq 0.15$, $\beta \simeq 3.4$, and $\gamma \simeq 1.2$.

Fig. 4 shows the histograms of the probabilities $\tilde{v} f_{\tilde{v}}$ for the velocity of escaped (at $\tilde{r}/\tilde{a} = 100$) and ejected (at $\tilde{r}/\tilde{a} \to \infty$) stars, where the probability density function (PDF) is $f_{\tilde{V}} \equiv f_{\tilde{V}}(\tilde{v})$, for q = 0.1 and a = 100. The distributions incorporate the presence of the binary SMBH potential only. The histogram for \tilde{v}_{100} has a local maximum at $\tilde{v}/v_{\rm bh} = 1/\sqrt{50}$ (the escape velocity at $\tilde{r}/\tilde{a} = 100$), which is the value marked by the leftmost red vertical line; all stars with velocities to the right of this line are unbound to the binary SMBH and contribute to the distribution for \tilde{v}_{∞} . For $\tilde{v} \gtrsim 1000$ km s⁻¹, the escaped and ejected histograms have identical shapes since the stellar kinetic energies are much larger than the potential energies. The two red vertical lines on the right give the range over which the histograms decrease by a power law $p = \gamma \tilde{v}^{\beta}$. The middle one shows $v_{\rm pl,1}/v_0 \simeq k_1 (q/(1+q))^{1/2} (\tilde{a}/\tilde{r}_{\rm t1})^{-1/2}$, where k_1 is a constant in the range $1 \lesssim k_1 \lesssim 2$; this is simply an order-unity multiple of the velocity of the reduced mass, $\tilde{v} = (G\mu/\tilde{a})^{1/2}$, as it occurs slightly above the peak, which roughly coincides with the

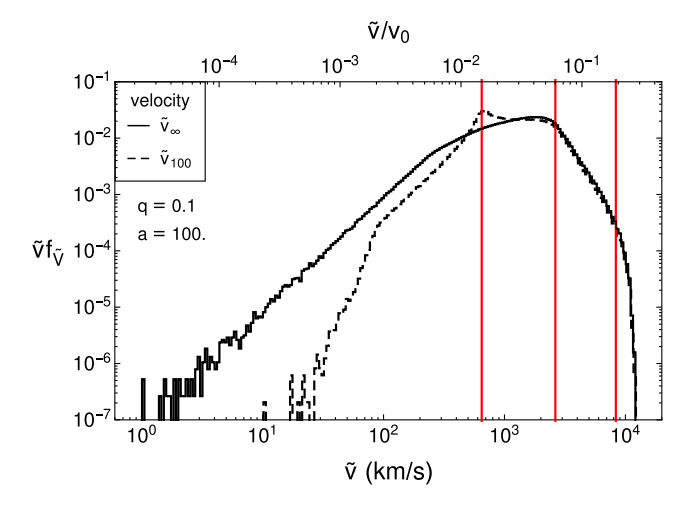


Figure 4. The probabilities $\tilde{v}f_{\tilde{V}}$ for q=0.1 and $a=\tilde{a}/\tilde{r}_{t1}=100$, for the velocity \tilde{v}_{∞} of ejected stars at $\tilde{r}/\tilde{a}\to\infty$ (solid) and the velocity \tilde{v}_{100} of escaped stars at $\tilde{r}/\tilde{a}=100$ (dashed), where the PDF is $f_{\tilde{V}}\equiv f_{\tilde{V}}(\tilde{v})$. The logarithmic bin widths are $\Delta_{\tilde{v}}=0.02$. From left to right, the red vertical lines show $\tilde{v}/v_{bh}=1/\sqrt{50}$ (the escape velocity at $\tilde{r}/\tilde{a}=100$); $v_{pl,1}/v_0\simeq k_1(q/(1+q))^{1/2}(\tilde{a}/\tilde{r}_{t1})^{-1/2}$ where $1\lesssim k_1\lesssim 2$ (slightly above the peak, the start of the decreasing power-law region); and $v_{pl,2}/v_0\simeq k_2(1/(1+q))^{1/2}(\tilde{a}/\tilde{r}_{t1})^{-1/2}$, where $1\lesssim k_2\lesssim 2$ (the end of the decreasing power-law region). Here, $k_1=k_2=2$.

mean. The right one shows $v_{\rm pl,\,2}/v_{\rm bh}\simeq k_2(1/(1+q))$ (or equivalently, $v_{\rm pl,\,2}/v_0\simeq k_2(1/(1+q))^{1/2}(\tilde{a}/\tilde{r}_{\rm tl})^{-1/2})$, where k_2 is a constant in the range $1\lesssim k_2\lesssim 2$; this is simply an order-unity multiple of the velocity of the secondary, $\tilde{v}/v_{\rm bh}=1/(1+q)$, which is the largest velocity scale in the system. These features and the locations quoted here apply over our entire parameter range, as presented below.

Fig. 5(a) shows the probabilities for the velocity \tilde{v}_{∞} of ejected stars (at $\tilde{r}/\tilde{a} \to \infty$ in the presence of the binary SMBH potential only) for a = 100. The peak shifts by about an order of magnitude with a 2 orders of magnitude change in the mass ratio. The shapes of the distributions depend on the mass ratio. For q = 1, there is an abrupt drop after the peak of the distribution; the power-law region becomes vanishingly small (since $v_{\rm pl,\,1} \simeq v_{\rm pl,\,2}$), and the peak is close to the maximum velocity and considerably higher than the mean in Fig. 3. As q decreases, there is a more gradual decline from the peak to the maximum velocity; the power-law region is larger and the peak is closer to the mean. This trend occurs because lower mass ratio SMBH binaries have lower reduced mass velocities and thus impart less energy to the ejected stars on average, but they have higher secondary velocities and can thus still eject stars to high velocities after close encounters. The red curves show $p = \gamma \tilde{v}_{\infty}^{\beta}$ fit to the power-law region defined above; the specific values of γ and β are not particularly illuminating, so we do not present them.

Fig. 5(b) shows the probability distributions for q=0.1. The peak again shifts by about an order of magnitude with a 2 order of magnitude change in the separation. The histograms have similar shapes, merely shifted along the v-axis for different a. Indeed, the histograms coincide when plotted in the units $\tilde{v}_{\infty}/v_{\rm bh}$, apart from a slightly lower maximum velocity for a=10. The distributions for the other values of q exhibit this behaviour as well.

The similarity in the histograms for different a is a result of the scale invariance with respect to a in our simulation set-up and the small tidal disruption probability over our parameter range. The small deviation for a = 10 arises because the tidal disruption probability is higher at this separation (Darbha et al. 2018). Stars

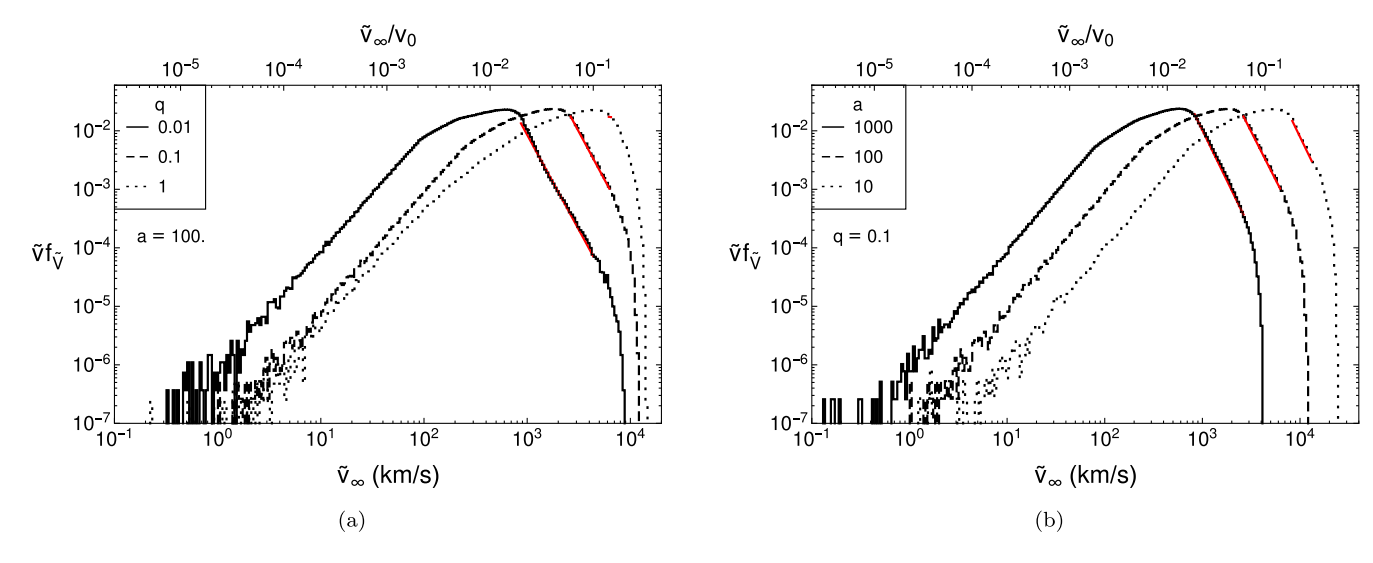


Figure 5. (a) The probabilities $\tilde{v}f_{\tilde{V}}$ for the velocity \tilde{v}_{∞} of ejected stars at $\tilde{r}/\tilde{a} \to \infty$, where the PDF is $f_{\tilde{V}} \equiv f_{\tilde{V}}(\tilde{v})$, for $a = \tilde{a}/\tilde{r}_{t1} = 100$ and q = 0.01 (solid), 0.1 (dashed), and 1 (dotted). (b) The probabilities for q = 0.1 and $a = \tilde{a}/\tilde{r}_{t1} = 1000$ (solid), 100 (dashed), and 10 (dotted). The logarithmic bin widths are $\Delta_{\tilde{v}} = 0.02$. The red curves show the power law $p = \gamma \tilde{v}_{\infty}^{\alpha}$ fit to the regions $k_1(q/(1+q))^{1/2}(\tilde{a}/\tilde{r}_{t1})^{-1/2} \lesssim \tilde{v}_{\infty}/v_0 \lesssim k_2(1/(1+q))^{1/2}(\tilde{a}/\tilde{r}_{t1})^{-1/2}$, where $1 \lesssim k_1, k_2 \lesssim 2$.

incident with low angular momenta are both preferentially disrupted (Coughlin et al. 2017) and preferentially ejected with high velocities since they experience close encounters with the binary SMBH. Since an integration terminates when a star is disrupted, the higher disruption probability implies that fewer low angular momentum stars are available to undergo high-velocity ejections. This deviation is thus physical, and we expect to observe it in realistic velocity spectra.

We compare our results in Fig. 5 to the velocity distributions found by Sesana et al. (2006) for circular SMBH binaries, and find rough agreement. We cannot make a direct comparison, since we have a different criterion for an 'ejection,' as noted earlier, and we plot the probability whereas they plot the PDF. However, we can still roughly compare the features that are revealed despite these different approaches. In both works, the distributions have similar high-velocity ranges; they have high-velocity regions that are well described by a decreasing power law, and this region is larger for lower mass ratios (Sesana et al. 2006 use a broken power law to fit a larger region than we do, so here we are referring to the highvelocity region after the break); and the velocity distributions at the escape sphere (shown in this work by the curves for \tilde{v}_{100} in Figs 4 and 6) achieve a maximum at the velocity corresponding to the incident energy, which arises from the stars that are only lightly perturbed by the binary SMBH.

Fig. 6 shows the probability distributions for the velocity \tilde{v}_{100} of escaped stars (at $\tilde{r}/\tilde{a}=100$ in the presence of the binary SMBH potential only) for a=100. This radius for the escape sphere is less than or roughly equal to the influence radius of the binary SMBH and much less than any galactic length scales, and so these distributions hold regardless of the galactic potential or stellar distribution in the bulge. The shapes of the histograms change dramatically for different q, much more than those for \tilde{v}_{∞} . For q=1, the distribution is roughly flat for an order of magnitude change in \tilde{v}_{100} , and exhibits a double peaked structure at the two ends of this plateau, which correspond to the two red lines on the left in Fig. 4, and has a vanishingly small power-law region after the higher velocity peak. As q decreases, the lower velocity peak becomes more prominent,

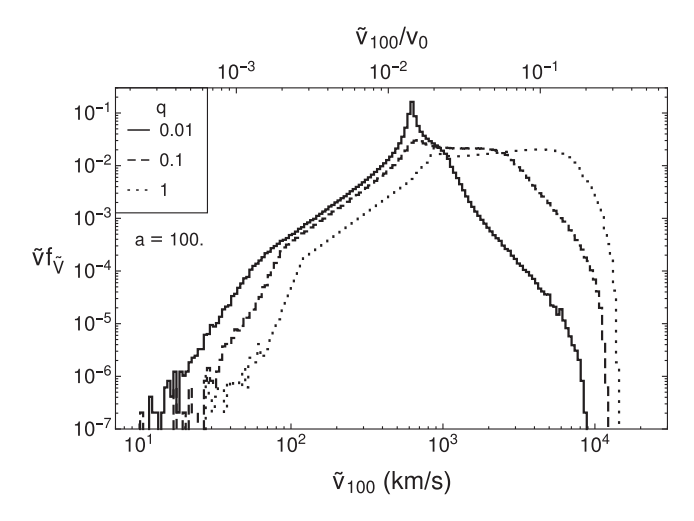


Figure 6. The probabilities $\tilde{v}f_{\tilde{V}}$ for the velocity \tilde{v}_{100} of escaped stars at $\tilde{r}/\tilde{a}=100$, where the PDF is $f_{\tilde{V}}\equiv f_{\tilde{V}}(\tilde{v})$, for $a=\tilde{a}/\tilde{r}_{t1}=100$ and q=0.01 (solid), 0.1 (dashed), and 1 (dotted). The stars with velocities $\tilde{v}_{100}\lesssim v_0\sqrt{(1+q)/50a}$ are bound to the binary SMBH and will not be ejected to infinity; this velocity corresponds to the position of the lower velocity peak. The logarithmic bin widths are $\Delta_{\tilde{v}}=0.02$.

the plateau shrinks, and the power-law region grows. For q=0.01, the lower velocity peak dominates since the low-mass secondary tends to only lightly perturb the incident stars from their $\epsilon=0$ orbits into mildly bound or unbound orbits, which results in the stellar velocities at $\tilde{r}/\tilde{a}=100$ clustering around the escape velocity. For a given q, the histogram has the same shape for different a, simply shifted along the \tilde{v} -axis as in Fig. 5(b).

Fig. 8(a) shows the probability that an ejected star has a velocity at $\tilde{r}/\tilde{a} \to \infty$ of $\tilde{v}_{\infty} > v_{\rm c}$, where $v_{\rm c}$ is a cut-off velocity, for q=0.1. The curves are very similar, simply shifted along the $v_{\rm c}$ -axis, due to the similarity in the underlying distributions (Fig. 5). If we consider a cut-off velocity like $v_{\rm c} \sim 1000\,{\rm km\,s^{-1}}$, then we see similar trends as in the mass ejection rates found by Quinlan (1996) and Sesana

et al. (2006). Fig. A2 shows the probabilities for different values of q in our parameter space.

3.2.2 Angular distribution

We parametrize the angle of the ejected stars with the direction cosine $\mu = \cos\theta = v_{z,\,\infty}/v_{\infty}$, where θ is the polar angle measured from the direction normal to the binary SMBH orbital plane. For an isotropic distribution of ejection directions, μ has a uniform PDF $f_M = 1/2$ for $-1 \le \mu \le 1$; note that in this case θ has a PDF $f_{\Theta} = (\sin\theta)/2$ for $0 \le \theta \le \pi$. The ejected stars are uniformly distributed in the azimuthal angle ϕ when ejected by a circular binary with a randomized phase, so we ignore this distribution. We calculate the angular distributions subject to different velocity cut-offs v_c .

Fig. 7 shows the histograms of the probabilities μf_M , where $f_M \equiv f_M(\mu)$ is the angular PDF, for q=0.1 and two different velocity cut-offs; Fig. A1 shows this for different values of q. If we examine a fixed cut-off $v_c \gtrsim 200\,\mathrm{km\,s^{-1}}$, then we see a clear trend: for a fixed mass ratio, tighter circular SMBH binaries eject stars more isotropically, whereas wider ones eject them more in the binary SMBH orbital plane; similarly, for a fixed separation, unequalmass circular binaries (i.e. IMBH/SMBH binaries) eject stars more in the orbital plane, whereas nearly equal-mass ones eject them more isotropically. Sesana et al. (2006) found the same trend that we observe for fixed q and changing q; we cannot directly compare to their results for eccentric binary SMBHs for fixed q and changing q. Any difference that might arise in the latter case would be due to the difference in our set-ups, as described previously (Sections 2).

Fig. 8(b) shows the normed mean direction of the ejected stars with velocity $\tilde{v}_{\infty} > v_{\rm c}$ for q = 0.1; Fig. A2 expands this to the other q in our parameter space. For a sufficiently high cut-off, a binary SMBH preferentially emits stars near its orbital plane, with higher cut-offs needed for tighter binaries and higher mass ratios. However, this trend is not quite monotonic with velocity for a fixed q and a. The curves exhibit a small bump towards more isotropic emission in a region around $v_{\text{pl},1}/v_0 \simeq k_1 (q/(1+q))^{1/2} (\tilde{a}/\tilde{r}_{t1})^{-1/2}$, shown by the middle red vertical line in Fig. 4, where the size of the region correlates with the size of the power-law region of the underlying velocity distribution. This suggests that the stars with velocities just after the peaks are preferentially emitted near the orbital plane. There is also a spike at high velocities, though this is likely due to noise from the low statistics there. These two features can in principle be used to constrain the binary SMBH mass ratio and separation.

3.3 Time-dependent ejection rate

In this subsection, we present the time-dependent ejection rate of hypervelocity stars by a binary SMBH contracting due to stellar scattering and gravitational wave emission. We examined the time-dependent tidal disruption rate in Darbha et al. (2018); for a more detailed discussion of the dynamics of the inspiral, we refer the reader there (or to earlier work by Zier & Biermann 2001). Here, we briefly summarize our set-up and modify it to describe HVSs.

We use the units $G = M_1 = \tilde{r}_{t1} = 1$ to write the dimensionless binary SMBH separation a and the stellar specific energy ε and angular momentum ℓ . We define the time-scale

$$t_0 = \frac{\tilde{r}_{11}^4 c^5}{G^3 M_1^3} \simeq 7.7 \times 10^{-1} \text{y} \left(\frac{M_1}{10^6 \,\text{M}_\odot}\right)^{-5/3} \left(\frac{M_*}{\text{M}_\odot}\right)^{-4/3} \left(\frac{R_*}{\text{R}_\odot}\right)^4$$
(5)

to define the dimensionless time $t = \tilde{t}/t_0$. We consider a primary mass $M_1 = 10^6 \, \mathrm{M}_{\odot}$ and stars with solar parameters in what follows. In these units, the total inspiral rate is

$$\frac{\mathrm{d}a}{\mathrm{d}t} = \left(\frac{\mathrm{d}a}{\mathrm{d}t}\right)_{\mathrm{ss}} + \left(\frac{\mathrm{d}a}{\mathrm{d}t}\right)_{\mathrm{gw}}.\tag{6}$$

The rate of coalescence due to gravitational wave (gw) emission by two-point particles on a circular orbit is (Peters 1964)

$$\left(\frac{\mathrm{d}a}{\mathrm{d}t}\right)_{\mathrm{ow}} = -\frac{64}{5} \frac{q(1+q)}{a^3}.\tag{7}$$

The inspiral rate due to stellar scattering (ss) is

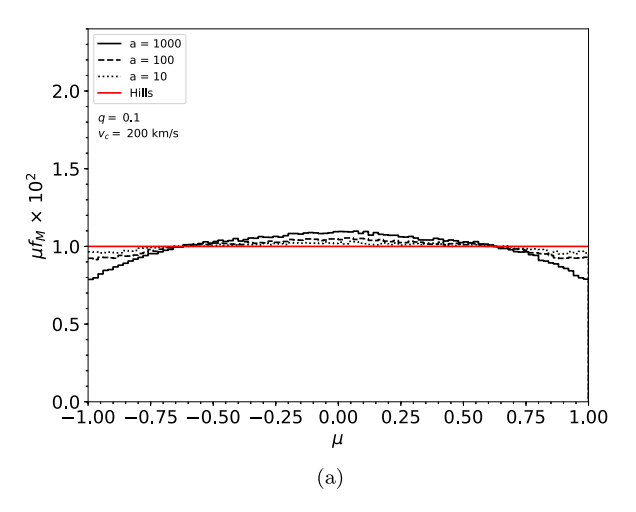
$$\left(\frac{\mathrm{d}a}{\mathrm{d}t}\right)_{\mathrm{ss}} = -\frac{2M_*}{M_1}\phi t_0 \frac{a^2}{q} \langle \Delta \epsilon_* \rangle (q, a) \lambda_{\mathrm{ej}}(q, a), \tag{8}$$

where $\langle \Delta \epsilon_* \rangle$ is the average change in the specific energy of the ejected stars and $\lambda_{\rm ej}$ is the stellar ejection probability, both found from our simulations; M_*/M_1 is the ratio of the stellar mass to the primary mass; and ϕ is the stellar injection rate from the binary SMBH loss cone (in units of yr⁻¹). This is simply $\phi(q, a) = 2a(1+q)\phi_0$, assuming the stars are incident from a full loss cone repopulated through two-body relaxation and are thus uniformly distributed in ℓ^2 (Frank & Rees 1976; Lightman & Shapiro 1977; Cohn & Kulsrud 1978; Magorrian & Tremaine 1999), where $\phi_0 \sim 10^{-4} \ \rm yr^{-1}$ is the fiducial rate for an SMBH of mass $M_{\bullet} = 10^6 \ \rm M_{\odot}$ (Magorrian & Tremaine 1999; Wang & Merritt 2004; Stone & Metzger 2016). The time-dependent ejection rate for stars with $\tilde{v}_{\infty} > v_c$ is then $\dot{n}_{\rm ej}(\tilde{v}_{\infty} > v_c) = \phi \lambda_{\rm ej}(\tilde{v}_{\infty} > v_c)$, where $\lambda_{\rm ej}(\tilde{v}_{\infty} > v_c)$ depends on q and a. We calculate a(t) and $\dot{n}_{\rm ej}$ as the binary SMBH contracts from a = 1000 ($\tilde{a} = 2.3 \ \rm mpc$) to 10 ($\tilde{a} = 0.023 \ \rm mpc$).

Fig. 9 shows $\dot{n}_{\rm ej}$ for stars with different velocity cut-offs $v_{\rm c}$. The rates are in the range $\sim 10^{-3}$ – 10^{-1} yr $^{-1}$ for q=1, and drop to $\sim 10^{-6}-10^{-3}$ yr $^{-1}$ for q=0.01. The SMBH binaries eject a burst of stars with $\tilde{v}_{\infty}\gtrsim 3000$ km s $^{-1}$ as they are about to coalesce, for our full range of mass ratios. For $v_{\rm c}\simeq 1000$ km s $^{-1}$, the ejection rate actually declines monotonically for binaries with high mass ratios ($q\gtrsim 0.2$), and only those with low mass ratios ($q\lesssim 0.05$) exhibit a burst at late times. The ejection rate transitions between these two phases at $v_{\rm c}\simeq 2000$ km s $^{-1}$, where the rate remains roughly constant over the binary SMBH lifetime for $q\gtrsim 0.5$.

This behaviour arises due to a trade-off: as the SMBH binary contracts, it ejects higher velocity stars (Figs 5, A2), but when gravitational radiation begins to dominate, the binary ejects fewer stars overall since it contracts more rapidly and spends less time at a given separation (equation 7). For low mass ratios, the first effect is dominant; a q=0.01 SMBH binary at a=1000 ejects few stars with velocities $\tilde{v}>v_c\sim 1000$ km s⁻¹ (Fig. A2), but as it contracts, it ejects more stars above this cut-off, larger than the number suppressed by the gravitational wave coalescence. For nearly equalmass ratios, the second effect is dominant; a q=1 SMBH binary at a=1000 already ejects most stars with velocities $\tilde{v}>v_c\sim 1000$ km s⁻¹ (Fig. A2), and though it ejects slightly more in this range as the binary SMBH contracts, the rapid coalescence suppresses the possibility of ejections, and the ejection rate decreases.

A burst thus arises as a result of the decreasing binary SMBH separation alone, in a time $\tilde{t}\sim 10-100$ Myr, given that stars are continually injected from a full loss cone. Earlier work hinted at this result (Sesana et al. 2006), though here we explicitly fold in the SMBH binary coalescence rate, which washes out the effect for nearly equal-mass binaries when $v_{\rm c}=1000\,{\rm km\,s^{-1}}$. Previous studies have calculated a burst of HVSs over the lifetime of a binary SMBH, but under different physical conditions. A stable binary SMBH that



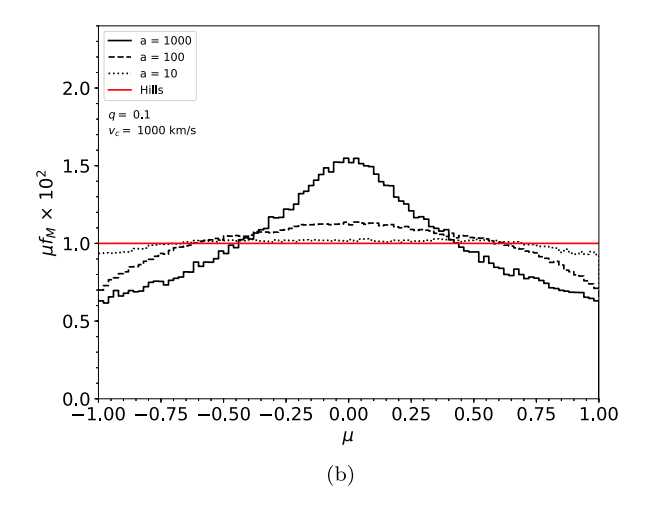


Figure 7. The probabilities μf_M for the direction cosine $\mu = \cos\theta = v_{z,\infty}/v_{\infty}$ of ejected stars at $\tilde{r}/\tilde{a} \to \infty$, for q=0.1 and $a=\tilde{a}/\tilde{r}_{t1}=1000$ (solid), 100 (dashed), and 10 (dotted). The PDF is $f_M \equiv f_M(\mu)$. The variable θ is the polar angle measured from the direction normal to the binary SMBH orbital plane. The panels show the distributions after applying the velocity cut-offs $\tilde{V} > v_c$, where v_c is (a) $200 \, \mathrm{km \, s^{-1}}$ and (b) $1000 \, \mathrm{km \, s^{-1}}$. The linear bin widths are $\Delta_{\mu} = 0.02$. The red curve shows the uniform distribution for μ produced by the Hills mechanism.

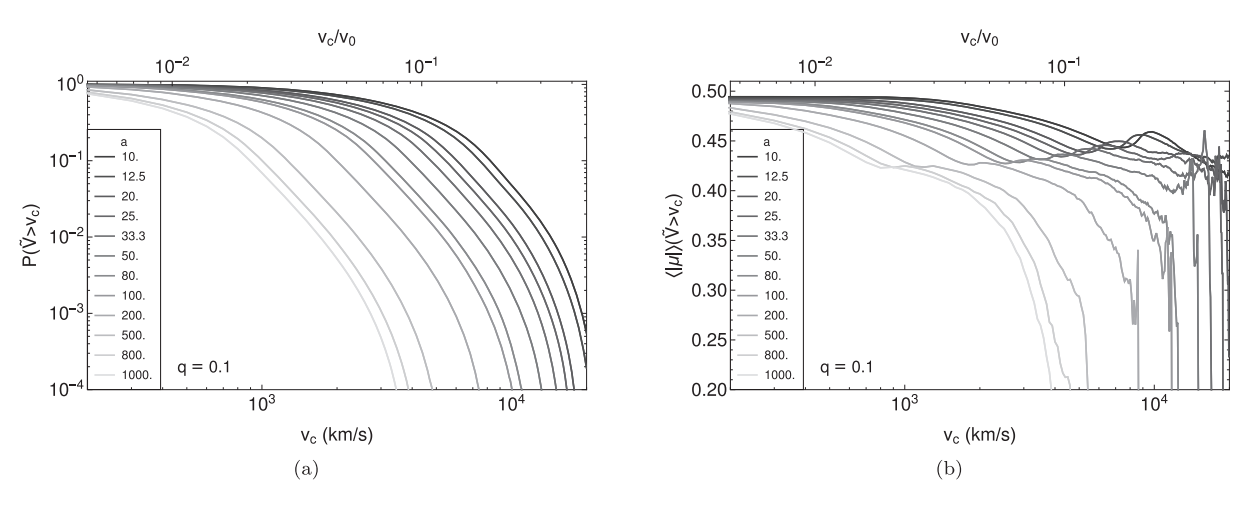


Figure 8. Statistics of ejected stars with a range of velocity cut-offs v_c , for q=0.1. (a) The probability $P(\tilde{V}>v_c)$ that an ejected star has a velocity at $\tilde{r}/\tilde{a}\to\infty$ of $\tilde{v}_\infty>v_c$. (b) The orientation of ejected stars with velocities $\tilde{v}_\infty>v_c$. The orientation is parametrized by $\mu=\cos\theta=v_{z,\infty}/v_\infty$, where θ is the polar angle measured from the direction normal to the binary SMBH orbital plane. For an isotropic distribution, $\langle |\mu| \rangle = 0.5$.

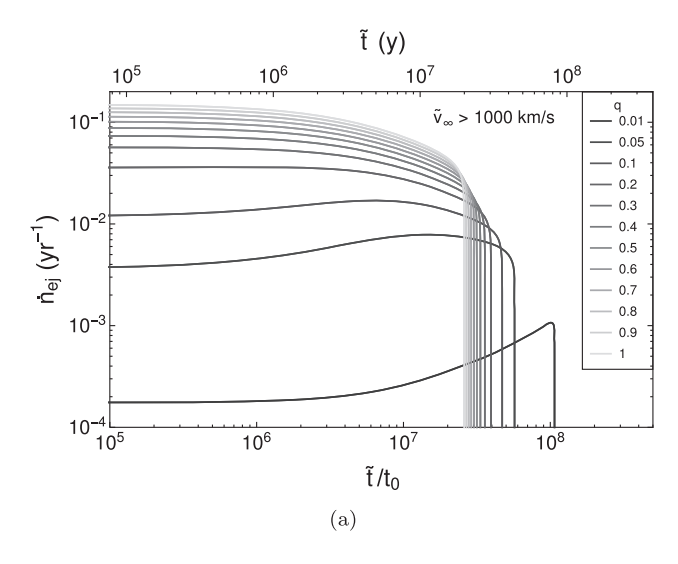
ejects incident unbound stars will produce a surge of HVSs when the binary first becomes hard and expels the stars present in the loss cone (Sesana et al. 2007b). An IMBH, inspiraling through a stellar cusp due to dynamical friction, can also produce a burst when it reaches the centre where the cusp is most dense, promptly ejecting the high concentration of stars and leaving behind a depleted region (Baumgardt et al. 2006; Levin 2006; Sesana et al. 2008).

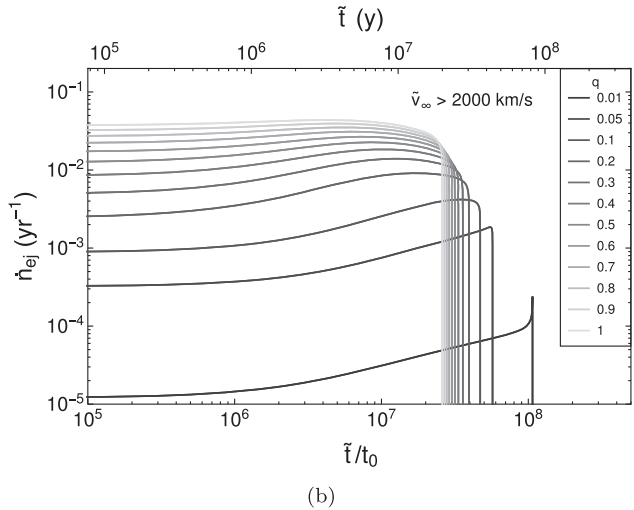
4 COMPARISON WITH THE HILLS MECHANISM

Hypervelocity stars exhibit different properties depending on the mechanism by which they are produced, and can thus reveal information about possible massive BH binarity and the distribution of stars in a galactic nucleus. Here, we compare the distributions of HVSs ejected by a single and binary SMBH. We first calculate the integrated distributions for the two production mechanisms with different parameters (Section 4.1), and then use parameter estima-

tion to study the number of samples required to distinguish between them (Section 4.2).

To study the properties of HVSs ejected by the Hills mechanism (Hills 1988), we simulated 2×10^5 encounters between a binary star and an isolated SMBH using the N-body code REBOUND with the IAS15 integrator (Rein & Liu 2012; Rein & Spiegel 2015). Due to scale invariance, we ran our simulations with the simulation parameters in the units $G = m_{\text{tot}} = \tilde{a}_* = 1$, where $m_{\text{tot}} = m_1 + m_2$ is the total mass of the binary star system with primary (secondary) mass m_1 (m_2) and \tilde{a}_* is the incident binary star separation. We ran our simulations for Sun-like stars, $m_1 = m_2 = 1 \text{ M}_{\odot}$, and a BH of mass $M_{\bullet} = 10^6 \,\mathrm{M_{\odot}}$. The origin of the coordinate system was set to the three-body centre of mass. Each binary star was initialized with its centre of mass on a parabolic orbit at a distance of r = 2000 relative to the SMBH, and with an isotropically distributed orientation. The pericentre of the parabolic orbit was sampled uniformly in the interval $r_p \in [0, 175]$; we used a uniform distribution since we treated the binary loss cone in the 'pinhole' regime, and we set this range since the probability of a Hills ejection drops to zero for r_p





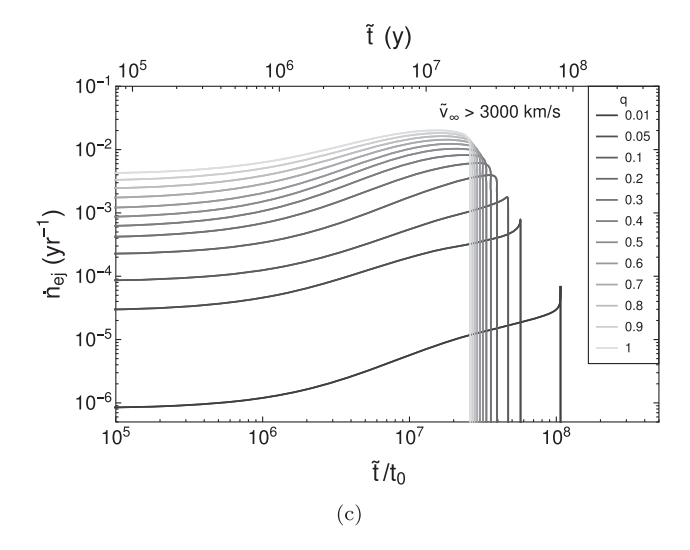


Figure 9. The time-dependent ejection rate $\dot{n}_{\rm ej}$ of stars with velocities $\tilde{v}_{\infty} > v_{\rm c}$, where $v_{\rm c}$ is (a) $1000~{\rm km\,s^{-1}}$, (b) $2000~{\rm km\,s^{-1}}$, and (c) $3000~{\rm km\,s^{-1}}$, for $M_1 = 10^6~{\rm M}_{\odot}$ and Sun-like stars, starting at an initial separation of $a = \tilde{a}/\tilde{r}_{\rm t1} = 1000~(\tilde{a} = 2.3~{\rm mpc})$.

 ≥ 175 (Hills 1988). We stopped the integration if a star escaped to r=4000 or if the simulation time reached $t=10^4$; we ignored the possibility of a tidal disruption as the probability of one is small (Mandel & Levin 2015). We classify an encounter as a Hills ejection if at least one of the stars crosses the escape sphere at r=4000, one star is unbound and the other is bound to the SMBH, and the stellar binary energy is positive (i.e. the two stars are on a relative unbound orbit). We only recorded ejected stars, so we do not need to distinguish between 'ejected' and 'escaped' stars here as we did for the SMBHB mechanism in Section 3.1. We find the same ejection probabilities versus pericentre distance as in previous studies, and the same mean ejected velocity of $\langle \tilde{v}_{\infty} \rangle \sim \tilde{a}_*^{-1/2} m_{tot}^{1/3} M_{\bullet}^{1/6}$, where M_{\bullet} is the black hole mass (Hills 1988; Bromley et al. 2006).

4.1 Integrated distributions

Although the average properties of ejected HVSs can constrain the nature of their progenitors (Section 3; Yu & Tremaine 2003; Gualandris et al. 2005), the distributions can reveal more complete information. In addition, HVSs observed at a given epoch were produced over an interval of time, and were thus likely sampled from an integrated PDF for each ejection mechanism. If the stars were ejected by the Hills mechanism, they were sampled from a PDF integrated over a range of incident binary star separations. If they were ejected by a binary SMBH, they may have been sampled from one integrated over the binary SMBH lifetime (Section 3.3). In particular, for the Milky Way, GC-origin HVSs observed with velocities $\tilde{v} \sim 1000 \, \mathrm{km \ s^{-1}}$ at Galactocentric distances $\tilde{r} \sim 100 \, \mathrm{kpc}$, roughly the current limit of HVS distance measurements (Boubert et al. 2018; Brown et al. 2018), would have been produced $t \sim$ 100 Myr ago (ignoring the Galactic potential). If there was a binary SMBH with separation $\tilde{a} \sim 2$ mpc in the GC in the recent past, then it would have coalesced in a time $T \sim 30-100$ Myr (Fig. 9), and the HVSs observed at large distances would have arisen from a PDF integrated over the binary SMBH lifetime. In contrast, if the binary SMBH had a larger separation, then it would contract more slowly and would not have coalesced in the past $t \sim 100$ Myr, and the HVSs observed would have arisen roughly from the PDF of a binary SMBH with a single set of parameters. The other local sources of HVSs have similar behaviour.

In previous work, authors have studied the integrated distributions in the context of an IMBH inspiraling towards an SMBH through a stellar cusp, both for the velocity (Baumgardt et al. 2006; Sesana et al. 2007a) and the ejection direction (Zier & Biermann 2001; Baumgardt et al. 2006; Levin 2006), and have compared these with the Hills mechanism. Here, we compare the integrated distributions produced by nearly equal-mass binary SMBHs that eject incident unbound stars with those produced by the Hills mechanism.

4.1.1 Velocity distribution

We first consider the velocity distribution of HVSs ejected by the Hills mechanism. To simplify our calculations, we define the dimensionless binary star separation $a_* = \tilde{a}_*/a_{*0}$, where the length scale $a_{*0} = 1$ au, and the dimensionless velocity $v = \tilde{v}/v_*$, where $v_*(a_*) = \sqrt{Gm_{\text{tot}}/\tilde{a}_*} = \sqrt{Gm_{\text{tot}}/a_*a_{*0}}$ is the characteristic circular velocity of a binary star with total mass m_{tot} and semimajor axis \tilde{a}_* , or dimensionally

$$v_* \simeq 133 \,\mathrm{km \, s^{-1}} \left(\frac{m_{\mathrm{tot}}}{2 \,\mathrm{M}_{\odot}}\right)^{1/2} \left(\frac{\tilde{a}_*}{0.1 \,\mathrm{au}}\right)^{-1/2}.$$
 (9)

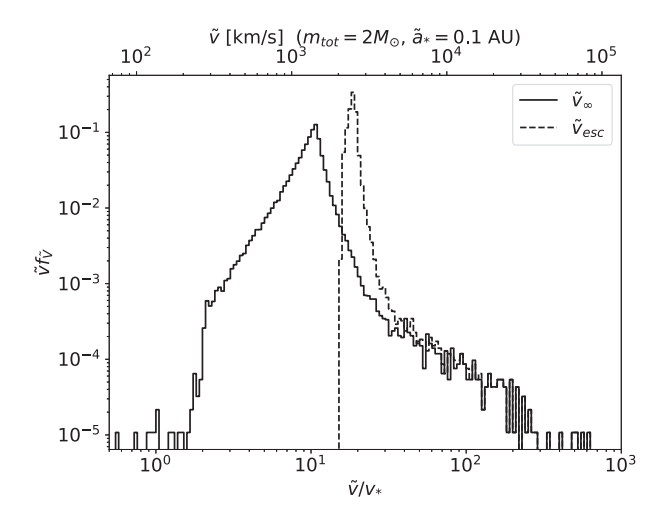


Figure 10. The probability distribution $\tilde{v} f_{\tilde{V}}$ for the velocity of stars ejected by the Hills mechanism at the escape sphere r=4000 (dashed) and at $r\to\infty$ (solid), where the PDF is $f_{\tilde{V}}\equiv f_{\tilde{V}}(\tilde{v}|\text{ej},a_*)$. The ratio of the black hole mass to the total stellar binary mass is $M_{\bullet}/m_{\text{tot}}=5\times10^5$. The upper \tilde{v} -axis gives the velocity in km s⁻¹ for a binary star with mass $m_{\text{tot}}=2\,\mathrm{M}_{\odot}$ and semimajor axis $\tilde{a}_*=0.1$ au.

The velocity PDF for ejected stars given an initial binary star separation a_* is $f_{\tilde{V}}(\tilde{v}|ej., a_*)$, where the random variable describing the end state is E = ej for an ejected star. This can be rewritten as $f_{\tilde{V}}(\tilde{v}|ei., a_*) = (1/v_*(a_*)) f_{V}(\tilde{v}/v_*(a_*)|ei., a_*)$. Due to scale invariance, the latter distribution simplifies to $f_V(\tilde{v}/v_*(a_*)|ej., a_*) =$ $f_V(\tilde{v}/v_*(a_*)|e_i)$, i.e. $v = \tilde{v}/v_*$ is conditionally independent of a_* given an ejection. Fig. 10 shows the velocity PDFs for Hills ejections at the escape radius and at $r \to \infty$, for a black hole mass $M_{\bullet}/m_{\text{tot}} =$ 5×10^5 . When the stars are infinitely far from the SMBH, the distribution is peaked at $v_{\infty} = \tilde{v}_{\infty}/v_{*} \simeq 10$ and decreases asymmetrically away from this point. This conforms to the data presented by Bromley et al. (2006), who approximate this central region in the v_{∞} distribution with a Gaussian. The mean velocity decreases by a factor of \sim 2 as the stars escape the gravitational potential of the black hole. The distribution is wider for v_{∞} since the v-axis is log-scaled, and thus the velocities in the central bin for $v_{\rm esc}$ get redistributed into a range of bins for v_{∞} .

The PDF for the ejected velocities integrated over a range of stellar binary separations is $f_{\tilde{V}}(\tilde{v}|ej) = \int f_{\tilde{V}}(\tilde{v}|ej, a_*) f_{A_*}(a_*) da_*$. The ejection probability is independent of a_* , $P(ej|a_*) = P(ej)$, due to scale invariance. In our model, the stellar binaries in the galactic bulge have semimajor axes distributed as $f_{A_*}(a_*) = K/a_*$ (Heacox 1998; Kobulnicky & Fryer 2007), i.e. a uniform distribution in $\log a_*$, where K is a normalization constant given by $K = [\ln(a_{*, \max}/a_{*, \min})]^{-1}$ for a minimum (maximum) separation of $a_{*, \min}$ ($a_{*, \max}$). The survivability of a binary star in three-body encounters in the bulge depends on the ratio of its circular velocity to the stellar velocity dispersion (Hills 1989), and the encounter rate (and thus the local stellar density). If $v_* \gtrsim \sigma$, where σ is the 1D stellar velocity dispersion, then the binary star's binding energy will likely increase in an encounter; if $v_* \lesssim \sigma$, then its binding energy will likely decrease in an encounter, either through the binary star widening or an exchange collision, ultimately leading to a dissociation after many such encounters. For a Milky Way-like galaxy, $\sigma \sim 100 \, \mathrm{km \, s^{-1}}$ (Gültekin et al. 2009), and the velocity condition roughly becomes $a_{*, \text{max}} \lesssim 0.1$ for binary stars with total mass $m_{\text{tot}} = 2 \,\mathrm{M}_{\odot}$. Many binary stars in the Galaxy have velocities less than σ due to the local density condition, so we take our upper bound to be slightly higher at $a_{*,\,\mathrm{max}}\simeq 1$, though the exact upper bound is unimportant since it simply translates into a different lower bound in the ejection velocities. If its separation becomes small, a stellar binary will undergo mass transfer or experience a merger, which imposes a rough lower bound $a_{*,\,\mathrm{min}}\gtrsim 0.001$. The integrated PDF is then

$$f_{\tilde{V}}(\tilde{v}|\mathrm{ej}) = K \int_{\ln a_{*,\mathrm{min}}}^{\ln a_{*,\mathrm{max}}} \frac{1}{v_{*}(a_{*})} f_{V}\left(\left.\frac{\tilde{v}}{v_{*}(a_{*})}\right| \mathrm{ej}\right) \mathrm{d}(\ln a_{*}). \tag{10}$$

Fig. 11(a) shows the integrated velocity distribution for stars ejected by the Hills mechanism for three different ranges of binary star separations. The lower the range of binary star separations can extend, the higher the ejected velocities can reach, as expected from energy conservation in the exchange collision. If the full range $a_{\ast} \sim 0.001-1$ of separations are possible, then the distribution becomes flat over $\tilde{v}_{\infty} \sim 10^3-10^4~{\rm km\,s^{-1}}$. Otherwise, it is flat over a smaller range of lower velocities.

The potential of the host galaxy can, of course, modify this distribution. Rossi et al. (2014) thoroughly studied the velocity distributions in the Galactic halo of HVSs ejected (presumably) by the Hills mechanism, including the contribution of the Galactic potential. As in this work, they initialized the stellar binaries with their centers of mass on parabolic orbits and uniformly distributed in r_p for the full loss cone regime (though they also studied the empty loss cone regime). The Authors considered the same distribution of binary star separations as in this work, $f_{\tilde{A}_*}(\tilde{a}_*) \sim 1/\tilde{a}_*$, though with $\tilde{a}_{*,\text{max}} \simeq 20 \text{ mpc} \ (\sim 4000 \text{ au}) \text{ and } \tilde{a}_{*,\text{min}} \simeq (1-10)R_*$ $(\sim 0.005 - 0.05)$ au for $R_* = R_{\odot}$). They studied two different distributions for the component masses. In the full loss cone regime, they find that the velocity peak occurs at $\tilde{v} \sim 800 \, \mathrm{km \, s^{-1}}$ for equal-mass stellar binaries with component masses $m_* = 3 \,\mathrm{M}_{\odot}$, which appears consistent with our result for $a_{*, min} = 0.01$ if we were to include deceleration from a galactic potential (most stars with $\tilde{a}_{*,\max} \gtrsim 1$ au would not escape the BH potential, so a different upper limit would not influence the peak location). In addition, they found that the velocity distribution before the peak depends solely on the Galactic potential, and after the peak on the properties of the stellar binaries. This suggests that we examine and compare the high-velocity regions of the velocity distributions, as they may encode information about the BH sources if the stellar populations are known.

We next turn to the velocity distribution of HVSs ejected by a binary SMBH. We write the dimensionless binary SMBH separation $a=\tilde{a}/\tilde{r}_{\rm tl}$, and define the dimensionless velocity $v=\tilde{v}/v_{\rm bh}$, where $v_{\rm bh}(q,a)=v_0\sqrt{(1+q)/a}$ is the characteristic binary SMBH circular velocity given in equation (3). The velocity distribution for a given binary SMBH mass ratio q and separation a can be expressed as $f_{\tilde{V}}(\tilde{v}|ej,q,a)$, where the random variable describing the end state is E=ej for an ejected star; Fig. 5 shows this distribution for several binary SMBH parameters.

To obtain an integrated PDF for the ejected velocities, we must integrate over the lifetime of the binary SMBH as it contracts. The details of the inspiral are given in Section 3.3. The integrated PDF for a given q is $f_{\tilde{V}}(\tilde{v}|ej,q)=f_{\tilde{V}EQ}(\tilde{v},ej,q)/f_{EQ}(ej,q)$, where $f_{\tilde{V}EQ}(\tilde{v},ej,q)=\int f_{\tilde{V}}(\tilde{v}|ej,q,a)P(ej|q,a)f_A(a|q)f_Q(q)da$ and $f(ej,q)=\int P(ej|q,a)f_A(a|q)f_Q(q)da$. The velocity distribution for a given q and a can be rewritten as $f_{\tilde{V}}(\tilde{v}|ej,q,a)=f_V(\tilde{v}/v_{bh}(q,a)|ej,q,a)/v_{bh}(q,a)$. Though we have the values of this distribution for the discrete values of a in our parameter space, we can obtain a continuous version in this case by approximating $f_V(\tilde{v}/v_{bh}(q,a)|ej,q,a)=f_V(\tilde{v}/v_{bh}(q,a)|ej,q,a)=100$, since the shape of $f_V(v|ej,q,a')$ is largely independent of a' (see

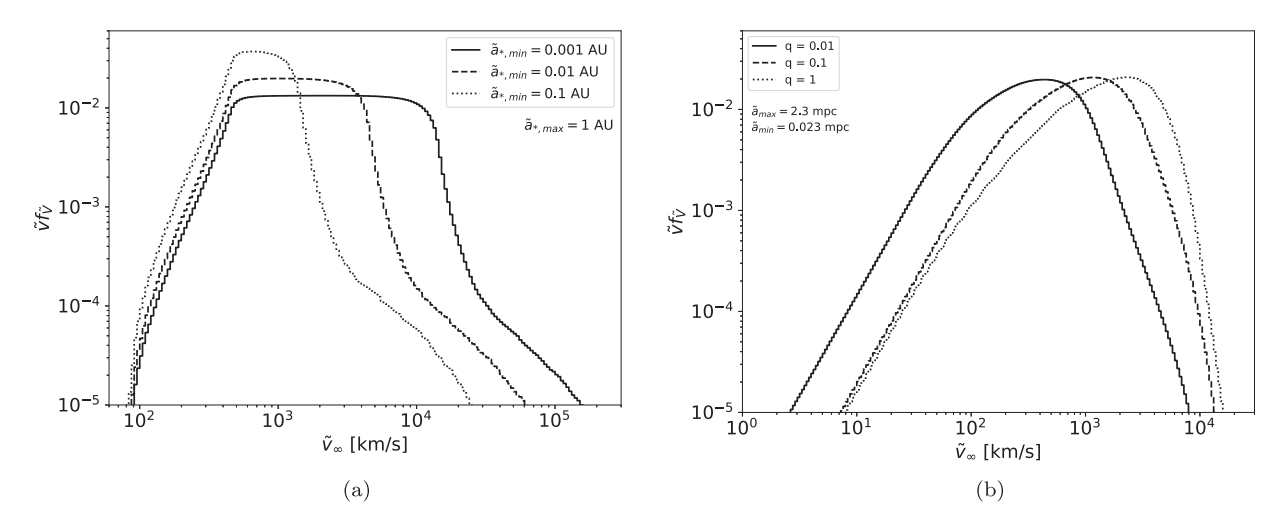


Figure 11. The integrated probability distributions $\tilde{v}_{f\tilde{v}}$ for the velocity \tilde{v}_{∞} of ejected stars. (a) The distributions for stars ejected by the Hills mechanism, using the BH mass $M=10^6\,\mathrm{M}_\odot$ and stellar masses $m_1=m_2=\mathrm{M}_\odot$. The incident binary stars are distributed in semi-major axis as $f_{\tilde{A}_*}(\tilde{a}_*)\sim 1/\tilde{a}_*$ between $\tilde{a}_{*,\mathrm{max}}=1$ au and $\tilde{a}_{*,\mathrm{min}}=0.001$ au (solid), 0.01 au (dashed), and 0.1 au (dotted). The integrated PDFs $f_{\tilde{V}}\equiv f_{\tilde{V}}(\tilde{v}|\mathrm{ej.})$ are given in equation (10). (b) The distributions for stars ejected by a binary SMBH contracting from $\tilde{a}_{\mathrm{max}}=2.3\,\mathrm{mpc}$ ($a_{\mathrm{max}}=1000$) to $\tilde{a}_{\mathrm{min}}=0.023\,\mathrm{mpc}$ ($a_{\mathrm{min}}=10$) due to stellar scattering and gravitational wave emission, using the primary mass $M_1=10^6\,\mathrm{M}_\odot$ and Sun-like stars, for q=0.01 (solid), 0.1 (dashed), and 1 (dotted). The integrated PDFs $f_{\tilde{V}}\equiv f_{\tilde{V}}(\tilde{v}|\mathrm{ej.},q)$ are given in equation (11).

Fig. 5 and the related discussion in the text). The ejection probability was previously labelled as $\lambda_{\rm ej}(q,a) \equiv P({\rm ej}|q,a)$ (Fig. 2). The PDF for the semi-major axis as the (circular) binary SMBH contracts is simply $f_A(a|q) = |({\rm d}t/{\rm d}a)_q|/T(q)$, where the binary SMBH lifetime is $T(q) = \int |({\rm d}t/{\rm d}a)_q| da$, and $({\rm d}t/{\rm d}a)_q$ is the inverse of the total contraction rate in equation (6). We integrate the distribution from $a_{\rm max} = 1000$ to $a_{\rm min} = 10$. The integrated PDF is then

$$f_{\tilde{V}}(\tilde{v}|\text{ej},q) = \frac{\int_{\ln a_{\text{min}}}^{\ln a_{\text{max}}} \left[\frac{f_{V}\left(\frac{\tilde{v}}{v_{\text{bh}}(q,a)} \middle| \text{ej},q,a'=100\right)}{v_{\text{bh}}(q,a)} \right] g(\text{ej},q,a)ad(\ln a)}{\int_{\ln a_{\text{min}}}^{\ln a_{\text{max}}} g(\text{ej},q,a)ad(\ln a)}$$

$$(11)$$

where $g(ej, q, a) \equiv \lambda_{ej}(q, a) \left| \left(\frac{dr}{da} \right)_q \right|$. We note that the p(q) terms and T(q) terms each cancelled out.

Fig. 11(b) shows the integrated velocity distribution of the ejected stars for three different values of q. The histograms are similar in shape, with the differences between them arising for the same reasons as in the underlying histograms for fixed separations (Fig. 5a). The distributions have a precise peak and a power-law decay away from the peak. Importantly, the binary SMBH coalesces rapidly by gravitational wave emission beginning around $a \sim 100$ (Darbha et al. 2018), so the high velocities found in the distributions for $a \lesssim 100$ are suppressed (Fig. 5b).

The distributions produced by a binary SMBH are distinct in shape from those produced by the Hills mechanism, although this may not fully persist when including the influence of the galactic potential (Rossi et al. 2014). In addition, for a binary SMBH with q=0.1-1 and a binary star distribution with $a_{*,\,\mathrm{min}}=0.01$, the two overlap and are difficult to distinguish. If stellar binaries in the bulge can shrink to $a_{*,\,\mathrm{min}}\sim0.001$, then they can reach much higher velocities than those produced by a binary SMBH; this high-velocity signature can thus reveal the presence of an isolated SMBH.

We compare our results to earlier studies, which calculated the velocity distributions as an IMBH inspirals through a stellar cusp towards an SMBH (Sgr A*, specifically) (Baumgardt et al. 2006; Sesana et al. 2007a). Their setups are very different from the scattering of unbound stars that we consider here, so we cannot make a direct comparison and do not expect similar outcomes, but a comparison can still highlight different features in the different scattering regimes.

In Baumgardt et al. (2006), the IMBH ($M_2 = 10^3 \,\mathrm{M}_{\odot} - 10^4 \,\mathrm{M}_{\odot}$) begins on a circular orbit about the SMBH ($M_1 = 3 \times 10^6 \,\mathrm{M}_{\odot}$) at $\tilde{a} = 100$ mpc and inspirals to $\tilde{a} \lesssim 1$ mpc. They find that the distributions drop off around $\tilde{v} \sim 2000 \, \mathrm{km \, s^{-1}}$ and are largely insensitive to the IMBH mass, and that the binary evolves to high eccentricities by the time it stalls if the IMBH mass is $M_2 \sim 10^4 \, \rm M_{\odot}$. In Sesana et al. (2007a), the IMBH (q = 1/729) begins on an eccentric orbit (e=0.9) at $\tilde{a}\sim 30$ mpc and inspirals until it stalls at $\tilde{a}\sim 4$ mpc. The Authors additionally fold in the influence of a model galactic potential; they find the distribution peaks at $\tilde{v}_{\infty} \sim 700 \text{ km s}^{-1}$. In contrast, our work examines the domain in which the central stellar density has been depleted and further contraction arises from stars incident from a full loss cone; for our primary mass $M_1 = 10^6 \,\mathrm{M}_{\odot}$, the binary SMBH begins at $\tilde{a} = 2.3$ mpc. In our work, for q = 0.01, we find a comparable distribtuion to the above works, with slightly lower ejection velocities. This suggests that it is difficult to use a HVS velocity spectrum to distinguish binary SMBHs in the early slingshot stage from those in the late slingshot stage with a full loss cone.

In the two studies above, the Authors also compared their results with distributions from the Hills mechanism. Baumgardt et al. (2006) analysed fixed stellar binary separations, and found that (for an SMBH with mass $M_{\bullet}=3.5\times10^6\,\mathrm{M}_{\odot}$) the distributions can be peaked at higher velocities than those from binary SMBHs if the stellar binaries are compact ($\tilde{a}_*\lesssim0.05~\mathrm{au}$). Sesana et al. (2007a) studied both flat and lognormal distributions for the stellar binaries, and found that the slope of the ejection velocity distribution is flatter for stars ejected by a SMBH-IMBH binary than those ejected by the Hills mechanism, and thus the SMBH-IMBH scenario favors higher velocities.

4.1.2 Angular distribution

We now calculate the integrated angular distribution from the two HVS ejection mechanisms. We calculate the distributions subject to different velocity cut-offs $v_{\rm c}$; we do this since an observed sample of ejected stars may exhibit such a cut-off due to the difficulty in observing low-velocity stars, particularly in the galaxy core where most are likely located, and since applying such cut-offs often yields distinguishing features.

For the Hills mechanism, isotropic incident stars produce isotropic ejected stars, and thus the angular PDF is $f_M(\mu|\text{ej}, \tilde{V} > v_\text{c}) = 1/2$ for all velocity cut-offs v_c and minimum binary star separations $a_{*,\,\text{min}}$. For the SMBHB mechanism, we calculate the integrated angular PDF $f_M(\mu|\text{ej},q,\tilde{V}>v_\text{c})$ using Bayesian inference, as we did with the velocity distributions in Section 4.1.1. We obtain

 $f_M(\mu|\text{ej}, q, \tilde{V} > v_c)$

$$= \frac{\int_{\ln a_{\min}}^{\ln a_{\max}} f_M(\mu|ej, q, a, \tilde{V} > v_c) h(ej, q, a, v_c) a d(\ln a)}{\int_{\ln a_{\min}}^{\ln a_{\max}} h(ej, q, a, v_c) a d(\ln a)}$$
(12)

where $f_M(\mu|\text{ej},q,a,\tilde{V}>v_c)$ is the angular PDF given that an ejection has occurred for a given q, a, and velocity cut-off $\tilde{V}>v_c$ (Fig. 7); $h(\text{ej},q,a,v_c) \equiv P(\tilde{V}>v_c|\text{ej},q,a)P(\text{ej},|q,a)f_A(a|q)$; $P(\tilde{V}>v_c|\text{ej},q,a)$ is the probability that a star has a velocity $\tilde{V}>v_c$ given that an ejection has occurred for a given q and q (Figs 8a and A2); and q (Fig. 4) and q (Figs 8a and A2); and q (Fig. 8a and Fig. 8a) and q (Fig. 8a) are the same as in Section 4.1.1 above. We evaluate this integral by discretizing it at the values of q in our parameter space.

Fig. 12 shows the integrated angular distribution for two different velocity cut-offs. For a given q, ejected stars are increasingly concentrated in the binary SMBH orbital plane as one applies higher cut-offs, where lower q require a lower cut-off to begin to see this effect, as we found for the distributions for fixed q and a (Section 3.2.2). Indeed, for a given q and v_c , the integrated distributions are very similar to the corresponding ones for a=100 (Figs 7 and A1). This is because $a\sim100$ is the closest separation at which the binary spends considerable time ejecting stars before rapidly coalescing by gravitational radiation (Darbha et al. 2018), and thus the separation that produces the largest deviation from isotropic emission.

Previous studies have examined some features of the ejection angles during the binary SMBH inspiral, but focused on a binary SMBH embedded in a stellar cusp (Zier & Biermann 2001; Baumgardt et al. 2006; Levin 2006), a different set-up from this work. The above Authors find different trends as compared to our work. Baumgardt et al. (2006) found that the ejected stars, with no velocity cut-off, are more isotropically distributed for a lower mass secondary SMBH, and exhibit an overdensity in the binary SMBH orbital plane for a higher mass secondary. Levin (2006) found that the ejected stars exhibit a small anisotropy as the binary shrinks.

4.2 Model fitting

In this subsection, we use Bayesian parameter estimation to calculate the number of HVS samples required to distinguish between the different integrated distributions, examining first the velocity distributions (Section 4.2.1) and second the angular distributions (Section 4.2.2). In what follows, we suppose that we have N samples of HVSs. Let the random variable D describe the class of distributions corresponding to a given SMBH progenitor, $D = \{d_{\text{smbhb}}, d_{\text{hills}}\}$. Let Θ label the parameter that parametrizes each class, so

that $\Theta = Q$ for $D = d_{\rm smbhb}$, and $\Theta = A_{*, \, \rm min}$ for $D = d_{\rm hills}$. Note that $f_{\Theta}(q \, | d_{\rm hills}) = f_{\Theta}(a_{*, \, \rm min} | d_{\rm smbhb}) = 0$. We drop the random variable $E = \rm ej$. We quantify the accuracy of a fit using the Bayesian odds ratio OR that our set of samples arises from one model $(d, \, \theta)$ as opposed to another $(d, \, \theta')$.

4.2.1 Estimation with velocity samples

We first consider the velocities $\tilde{V}_1, \ldots, \tilde{V}_N$ of the samples. The odds ratio OR given the observed velocities is

$$OR = \frac{f_{D,\Theta}(d,\theta|\tilde{v}_1,\ldots,\tilde{v}_N)}{f_{D,\Theta}(d',\theta'|\tilde{v}_1,\ldots,\tilde{v}_N)}$$
(13)

$$=\frac{f_{\tilde{V}_1,\dots,\tilde{V}_N}(\tilde{v}_1,\dots,\tilde{v}_N|d,\theta)f_{\Theta}(\theta|d)P(D=d)}{f_{\tilde{V}_1,\dots,\tilde{V}_N}(\tilde{v}_1,\dots,\tilde{v}_N|d',\theta')f_{\Theta}(\theta'|d')P(D=d')},$$
(14)

where $f_{\tilde{V}_1,\dots,\tilde{V}_N}(\tilde{v}_1,\dots,\tilde{v}_N|d,\theta)$ is the joint velocity PDF. The samples are independent, so $f_{\tilde{V}_1,\dots,\tilde{V}_N}(\tilde{v}_1,\dots,\tilde{v}_N|d,\theta)=f_{\tilde{V}_1}(\tilde{v}_1|d,\theta)\dots f_{\tilde{V}_N}(\tilde{v}_N|d,\theta)$, where $f_{\tilde{V}_i}(\tilde{v}_i|d,\theta)$ is the integrated PDF for a single sample (equation 10 and Fig. 11a for the Hills mechanism; equation 11 and Fig. 11b for the SMBHB mechanism). We have no prior knowledge about the SMBH progenitor, so $P(D=d_{\text{smbhb}})=P(D=d_{\text{hills}})=1/2$, and $f_{\Theta}(q|d_{\text{smbhb}})=f_{\Theta}(a_{*,\text{min}}|d_{\text{hills}})=1/3$ since we consider three discrete parameter values for each class. The odds ratio thus simplifies to

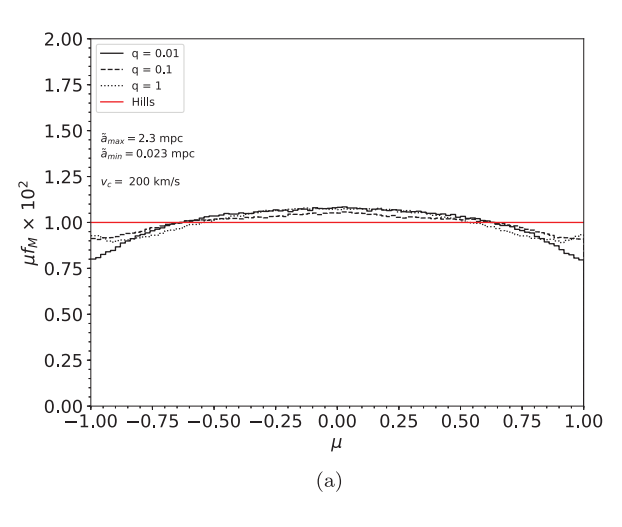
$$OR = \frac{f_{\tilde{V}_1}(\tilde{v}_1|d,\theta)\dots f_{\tilde{V}_N}(\tilde{v}_N|d,\theta)}{f_{\tilde{V}_1}(\tilde{v}_1|d',\theta')\dots f_{\tilde{V}_N}(\tilde{v}_N|d',\theta')}.$$
(15)

As discussed in Section 4.1, a sample of ejected stars may exhibit a velocity cut-off v_c . If we analyse HVSs with velocities $\tilde{V} > v_c$, then we can calculate the odds ratio as above by simply replacing the PDF for the full distribution d with that for the truncated distribution $d(\tilde{V} > v_c)$, namely $f_{\tilde{V}_i}(\tilde{v}_i|d,\theta) \to f_{\tilde{V}_i}(\tilde{v}_i|d(\tilde{V}_i > v_c),\theta) = f_{\tilde{V}_i}(\tilde{v}_i|d,\theta,\tilde{V}_i > v_c)$. The truncated PDF is

$$f_{\tilde{V}_i}(\tilde{v}_i|d,\theta,\tilde{V}_i>v_{\rm c}) = \begin{cases} \frac{f_{\tilde{V}_i}(\tilde{v}_i|d,\theta)}{1-F_{\tilde{V}_i}(v_{\rm c}|d,\theta)} &, \tilde{v}_i>v_{\rm c}\\ 0 &, \text{ else} \end{cases}$$
(16)

where $F_{\tilde{V}_i}(\tilde{v}|d,\theta) \equiv \int_{-\infty}^{\tilde{v}} f_{\tilde{V}_i}(\tilde{v}_i|d,\theta) d\tilde{v}_i$ is the cumulative distribution function (CDF), which is evaluated at v_c in the denominator. To simplify our calculation, we discretize our PDFs with the same logarithmic bin widths used in Fig. 11.

Fig. 13 shows the velocity-sampled odds ratio as a function of N for two different velocity cut-offs v_c , where the samples are drawn from the distribution $(D = d_{smbhb}, \Theta = Q = 0.1)$ and the odds ratio is calculated relative to this distribution. The true velocity distribution can be distinguished from the others most easily if the full distributions are known; in this case, only $N \sim 100$ samples are needed to obtain $OR \lesssim 10^{-6}$. In the intermediate range of cut-offs $200 \,\mathrm{km \, s^{-1}} \lesssim v_{\rm c} \lesssim 1000 \,\mathrm{km \, s^{-1}}$, roughly $N \sim 100 - 300 \,\mathrm{samples}$ are needed to distinguish $D = d_{\text{smbhb}}$ with q = 0.1 from $D = d_{\text{hills}}$ with $a_{*, \min} = 10^{-2}$, since these two distributions overlap heavily here (Fig. 11), but only $N \sim 50 - 100$ samples are needed to distinguish it from the other mechanisms. Sesana et al. (2007a) find that $N \ge 1$ 100 samples are needed to identify the ejection mechanism, and our numbers are in agreement for the above range of cut-offs. For $v_{\rm c}$ $\sim 2000 \, \mathrm{km \, s^{-1}}$, $N \sim 400 \, \mathrm{samples}$ are required to discriminate the SMBHB mechanism with different values of q, though only $N \sim$ 300 samples are needed to rule out the Hills mechanism. For $v_c \gtrsim$ 4000 km s⁻¹, the velocity distributions for the SMBHB mechanism with different q become very similar (Fig. 11b), and thousands of samples are needed to distinguish them.



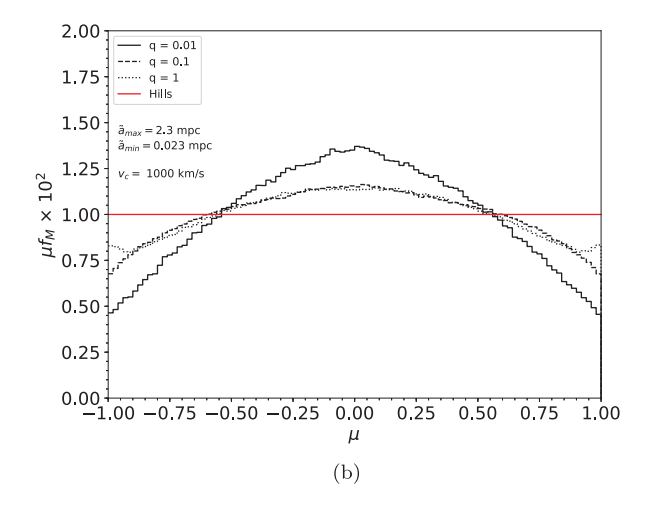
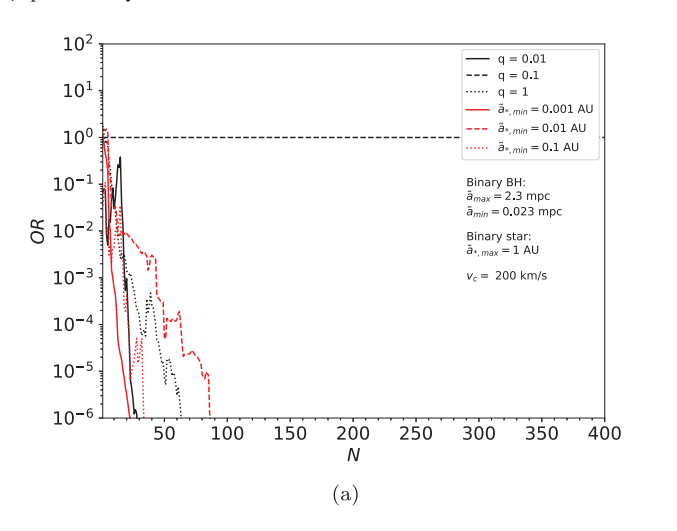


Figure 12. The integrated angular distributions $\mu f_{\rm M}$ for the direction cosine μ of stars ejected by the SMBHB mechanism with velocities $\tilde{V} > v_{\rm c}$, where the binary SMBH contracts from $\tilde{a}_{\rm max} = 2.3$ mpc ($a_{\rm max} = 1000$) to $\tilde{a}_{\rm min} = 0.023$ mpc ($a_{\rm min} = 10$) due to stellar scattering and gravitational wave emission. We consider a primary with mass $M_1 = 10^6 \, {\rm M}_{\odot}$ and Sun-like stars, and the mass ratios q = 0.01 (solid), 0.1 (dashed), and 1 (dotted). The velocity cut-offs $v_{\rm c}$ are (a) $200 \, {\rm km \, s^{-1}}$ and (b) $1000 \, {\rm km \, s^{-1}}$. The integrated PDFs $f_M \equiv f_M(\mu | {\rm ej}, q, \tilde{V} > v_{\rm c})$ are given in equation (12). The red curve shows the uniform distribution for μ produced by the Hills mechanism.



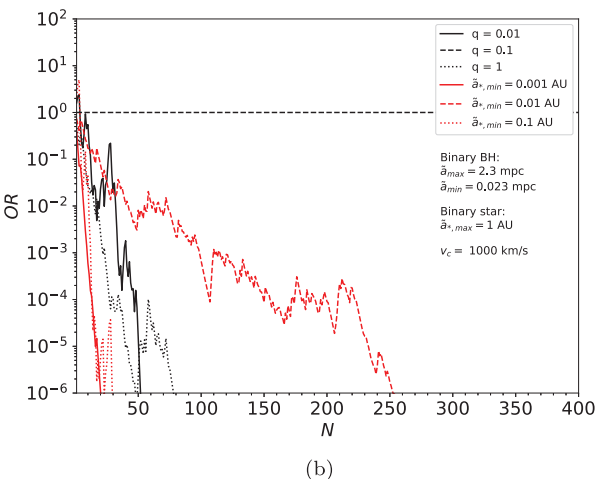


Figure 13. The velocity-sampled Bayesian odds ratio OR (equation 15) as a function of N randomly drawn samples. The samples were drawn from the distribution ($D = d_{\text{smbhb}}$, $\Theta = q = 0.1$), and the odds ratio for each distribution is calculated relative to it. The panels correspond to samples drawn from the truncated PDF with $\tilde{V}_i > v_c$, where v_c is a) $200 \, \text{km s}^{-1}$ and b) $1000 \, \text{km s}^{-1}$.

If the samples are drawn from $D=d_{\rm smbhb}$ with Q=0.01 or 1, then we find similar results of $N\sim$ hundreds of samples for $v_{\rm c}\lesssim 2000\,{\rm km\,s^{-1}}$, and $N\sim$ thousands for $v_{\rm c}\gtrsim 4000\,{\rm km\,s^{-1}}$. If the samples are drawn from $D=d_{\rm hills}$ with $A_{\rm *,min}=10^{-2}$, then we find analogous results to $D=d_{\rm smbhb}$ with $\Theta=Q=0.1$ for $v_{\rm c}\lesssim 1000\,{\rm km\,s^{-1}}$, though for $v_{\rm c}\gtrsim 2000\,{\rm km\,s^{-1}}$ only $N\sim 50-100$ samples are needed to distinguish this ejection mechanism from the others, since the high-velocity behaviour in Hills ejections is fairly distinct for a given minimum binary star separation.

4.2.2 Estimation with angular samples

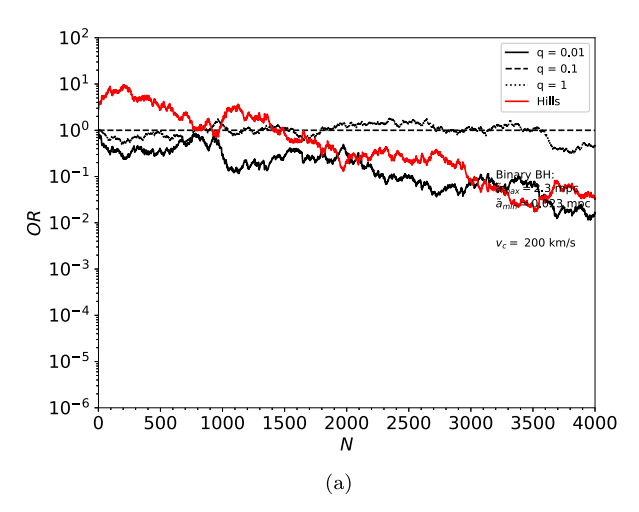
We next consider the direction cosines M_1, \ldots, M_N of the samples. We proceed as above, but set $f_{\Theta}(a_{*,\min}|d_{\text{hills}}) = 1$ here since the Hills mechanism ejects stars isotropically regardless of the minimum binary star separation. The odds ratio OR given the observed

directions is then

$$OR = \frac{f_{M_1}(\mu_1|d,\theta)\dots f_{M_N}(\mu_N|d,\theta)f_{\Theta}(\theta|d)}{f_{M_1}(\mu_1|d',\theta')\dots f_{M_N}(\mu_N|d',\theta')f_{\Theta}(\theta'|d')},$$
(17)

where $f_{M_i}(\mu_i|d,\theta)$ is the angular PDF for a single sample. If we generalize this by applying any velocity cut-off v_c , then the PDF is $f_{M_1}(\mu_1|d(\tilde{V}>v_c),\theta)=f_{M_1}(\mu_1|d,\theta,\tilde{V}>v_c)$ (equation 12 and the paragraph preceding it, and Fig. 12).

Fig. 14 shows the direction-sampled odds ratio as a function of N for two different velocity cut-offs, where the samples are drawn from the distribution ($D=d_{\rm smbhb}$, $\Theta=Q=0.1$) and the odds ratio is calculated relative to this distribution. The odds ratio calculated from the direction cosines requires many more samples to discriminate between the ejection mechanisms than that calculated from the velocity distribution. In general, thousands of samples are required regardless of v_c . For $v_c \lesssim 200 \, {\rm km \, s^{-1}}$, the distributions are all exactly or nearly isotropic, and require many thousands of samples to separate. As one examines increasingly higher velocity



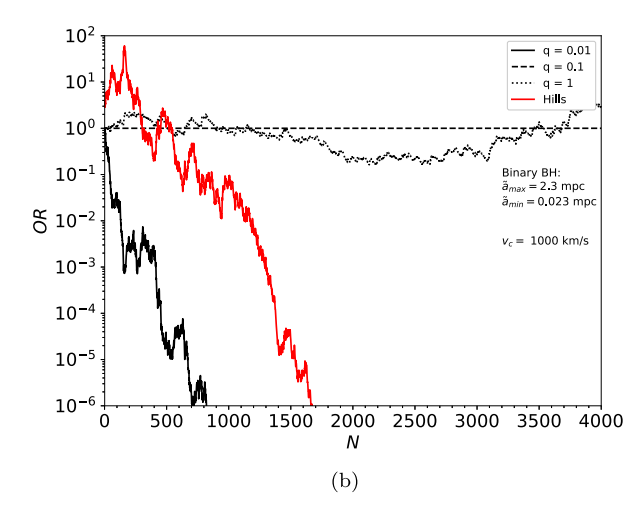


Figure 14. The direction-sampled Bayesian odds ratio OR (equation 17) as a function of N randomly drawn samples. The samples were drawn from the distribution ($D = d_{\text{smbhb}}$, $\Theta = q = 0.1$), and the odds ratio for each distribution is calculated relative to it. The panels correspond to samples drawn from the truncated PDF with $\tilde{V}_i > v_c$, where v_c is (a) $200 \, \text{km s}^{-1}$ and (b) $1000 \, \text{km s}^{-1}$.

cut-offs, fewer samples are needed to distinguish between the true distribution and some of the other distributions, but at a sufficiently high $v_{\rm c}$, the distributions for the different q all become peaked in the orbital plane and require many thousands of samples to separate. If the samples are drawn from $D=d_{\rm smbhb}$ with Q=0.01 or 1, then we find analogous results, albeit with different velocities at which the behaviour transitions. If the samples are drawn from $D=d_{\rm hills}$, then the behaviour is as expected: many thousands of samples are required for $v_{\rm c}\lesssim 200\,{\rm km\,s^{-1}}$, and the number of required samples decreases with increasing $v_{\rm c}$, reaching roughly $N\sim 1000$ samples for $v_{\rm c}\sim 2000\,{\rm km\,s^{-1}}$.

5 SUMMARY AND CONCLUSIONS

Galactic supermassive black holes can eject hypervelocity stars by several mechanisms, and the properties of the ejected stars can reveal information about their black hole progenitors and the galaxy in which they reside. In this paper, we studied encounters between unbound (parabolic, zero-energy) stars incident from a full loss cone and (hard, circular) binary SMBHs, and examined the properties of the ejected HVSs as a function of the binary SMBH mass ratio and separation. Where necessary, we considered a binary SMBH with primary mass $M_1 = 10^6 \, \mathrm{M}_\odot$ and an isolated SMBH with mass $M_{\bullet} = 10^6 \, \mathrm{M}_\odot$, and stars with solar parameters. We found several features of HVSs from binary SMBHs that both corroborate earlier work and reveal detailed behaviour:

- (1) The ejection probabilities are in the range $\lambda_{\rm ej}^{\rm bin} \simeq 0.5-0.86$, and are monotonically increasing functions of a and q (where $a=\tilde{a}/\tilde{r}_{\rm tl}$ is the dimensionless binary SMBH separation and $q=M_2/M_1$ is its mass ratio). The probabilities are largely independent of a for $a \gtrsim 100$, and of q for $q \gtrsim 0.2$. These are lower than the probabilities at which stars reach the escape sphere of our simulations, $\tilde{r}/\tilde{a}=100$, which roughly corresponds to the influence radius of the SMBHs.
- (2) The mean velocity of the stars ejected by a binary SMBH is well described by $\langle v_{\infty} \rangle \simeq \kappa v_0 (q/(1+q))^{1/2} (\tilde{a}/\tilde{r}_{t1})^{-1/2}$, where the constant of proportionality κ is q-dependent. We find it to be in the range $0.97 \le \kappa \le 1.06$ for our parameter space, which is less than the estimate $\kappa \simeq 1.8$ found by Yu & Tremaine (2003) (using $\langle v_{\infty} \rangle \simeq \sqrt{2\epsilon_{\infty}}$ and the numerical results of Quinlan 1996).

- (3) A binary SMBH preferentially emits stars near its orbital plane, where binaries with lower separations and higher mass ratios require higher velocity cut-offs to observe this effect (Figs 7 and A1); this trend is not monotonic, as the mean polar angle of ejected stars shows some bumps towards isotropy as a function of ejection velocity (Fig. 8b). The locations of these bumps suggest that stars are preferentially emitted near the orbital plane if they have velocities just after the peak of the velocity distribution (Fig. 5).
- (4) As the binary SMBHs in our parameter range contract, they eject stars with velocities $\tilde{v}_{\infty}\gtrsim 1000~{\rm km\,s^{-1}}$ at a rate $\sim 4\times 10^{-2}$ $-2\times 10^{-1}~{\rm yr^{-1}}$ for $q=1~(\sim 10^{-4}-10^{-3}~{\rm yr^{-1}}$ for q=0.01) (Fig. 9a). For our entire range of q, the binary SMBHs emit a burst of HVSs with $\tilde{v}_{\infty}>3000~{\rm km\,s^{-1}}$ as they are about to coalesce; for lower velocity cut-offs, only those with low mass ratios exhibit a burst at late times (Fig. 9).
- (5) The ejected star velocity distribution integrated over the lifetime of the ejecting binary SMBH has a well-defined peak and power-law decay away from the peak, in contrast to the generally flatter distribution for stars ejected by the Hills mechanism (integrated over typical binary star separations in the surrounding bulge) (Section 4). The former will yield lower velocities than the latter if the stellar binaries can reach a minimum separation of $\tilde{a}_{*,\min} \sim 0.001$ au; will be more difficult to distinguish if $\tilde{a}_{*,\min} \sim 0.01$ au; and will yield higher velocities if $\tilde{a}_{*,\min} \sim 0.1$ au (Fig. 11).
- (6) From a set of HVS samples, one can more efficiently identify the SMBH progenitor by performing parameter estimation using the sample velocities as opposed to the directions, and probing as much of the velocity distribution as possible (i.e. applying a velocity cut-off $\tilde{V} > v_{\rm c}$ with $v_{\rm c} \lesssim 200\,{\rm km\,s^{-1}}$). Roughly $N \sim 100$ samples are required when examining the velocities with $v_{\rm c} \lesssim 200\,{\rm km\,s^{-1}}$ (Fig. 13), whereas thousands of samples are required when examining the directions with any velocity cut-off (Fig. 14).

We focused on stars ejected directly by an SMBH progenitor, though HVSs (and more general 'runaway stars') can be produced through several other channels (Section 1). Of the many alternatives, only the star–BH cluster scenario can produce HVSs with velocities and at rates even approaching those of the Hills mechanism or a binary SMBH (Yu & Tremaine 2003; O'Leary & Loeb 2008). Indeed, the ejection rates by binary SMBHs that we find (Fig. 9)

are several orders of magnitude larger than those by star-BH cluster scattering found by O'Leary & Loeb (2008).

We analysed the ejection of incident unbound stars from a full loss cone. The details of the merger process may depopulate the loss cone in the far field, suppressing the rate of incident low angular momentum stars. The binary SMBH components will likely have bound stars at the earlier stage of the inspiral (Baumgardt et al. 2006; Sesana et al. 2008), so the absence of a full loss cone after the binary SMBH depletes the inner part of the cusp would make these bound stars the last source of HVSs.

We presented the velocities of ejected stars in the potential of the BH progenitors only. The shape of the galaxy can, of course, affect the properties of the ejected stars (Sesana et al. 2007a,b; Rossi et al. 2014). In particular, a galactic potential may homogenize some of the HVS properties, making it difficult to distinguish between different SMBH origins.

In Section 4, we compared HVSs arising from either single stars incident on a binary SMBH or binary stars incident on an isolated SMBH. In addition to these, if stellar binaries are incident on an SMBH binary, then one component of the SMBH binary can eject hypervelocity stars via the Hills mechanism (Coughlin et al. 2018). This additional process should be considered when examining the properties of HVSs to determine their SMBH progenitors; we leave this investigation to another paper.

Binary SMBHs can also eject hypervelocity binary stars (Lu, Yu & Lin 2007; Sesana, Madau & Haardt 2009; Coughlin et al. 2018; Wang et al. 2018). The stellar binaries typically depart with modified semimajor axes and increased eccentricities, and thus have a shorter merger time-scale than before the encounter (Coughlin et al. 2018). Isolated SMBHs can eject hypervelocity binary stars as well by disrupting stellar triple systems (Perets 2009; Fragione & Gualandris 2018). As with single HVSs, the properties of hypervelocity binary stars may depend on their origins and also serve as a probe of central black holes.

ACKNOWLEDGEMENTS

We thank Alberto Sesana for helpful clarifications, and the anonymous reviewer for helpful comments. This research used resources of the National Energy Research Scientific Computing Center, a Department of Energy Office of Science User Facility supported by the Office of Science of the U.S. Department of Energy under Contract No. DE-AC02-05CH11231. ERC was supported by the National Aeronautics and Space Administration through the Einstein Fellowship Program, Grant PF6-170150. This work was supported by the National Science Foundation under Grant No. 1616754. This work was supported in part by a Simons Investigator award from the Simons Foundation (EQ) and the Gordon and Betty Moore Foundation through Grant GBMF5076. Simulations in this paper made use of the REBOUND code which can be downloaded freely at http://github.com/hannorein/rebound.

REFERENCES

Arca Sedda M., Berczik P., Capuzzo-Dolcetta R., Fragione G., Sobolenko M., Spurzem R., 2017, preprint (arXiv:1712.05810)

Baumgardt H., Gualandris A., Portegies Zwart S., 2006, MNRAS, 372, 174

Blaauw A., 1961, Bull. Astron. Inst. Neth., 15, 265

Boubert D., Evans N. W., 2016, ApJ, 825, L6

Boubert D., Guillochon J., Hawkins K., Ginsburg I., Evans N. W., Strader J., 2018, MNRAS, 479, 2789 Bromley B. C., Kenyon S. J., Geller M. J., Barcikowski E., Brown W. R., Kurtz M. J., 2006, ApJ, 653, 1194

Brown W. R., 2015, ARA&A, 53, 15

Brown W. R., Anderson J., Gnedin O. Y., Bond H. E., Geller M. J., Kenyon S. J., 2015, ApJ, 804, 49

Brown W. R., Geller M. J., Kenyon S. J., Kurtz M. J., 2005, ApJ, 622, L33 Brown W. R., Lattanzi M. G., Kenyon S. J., Geller M. J., 2018, ApJ, 866, 9 Cohn H., Kulsrud R. M., 1978, ApJ, 226, 1087

Coughlin E. R., Armitage P. J., 2018, MNRAS, 474, 3857

Coughlin E. R., Armitage P. J., Nixon C., Begelman M. C., 2017, MNRAS, 465, 3840

Coughlin E. R., Darbha S., Kasen D., Quataert E., 2018, ApJ, 863, L24

Darbha S., Coughlin E. R., Kasen D., Quataert E., 2018, MNRAS, 477, 4009

Edelmann H., Napiwotzki R., Heber U., Christlieb N., Reimers D., 2005, ApJ, 634, L181

Erkal D., Boubert D., Gualandris A., Evans N. W., Antonini F., 2018, MN-RAS

Fragione G., Capuzzo-Dolcetta R., Kroupa P., 2017, MNRAS, 467, 451

Fragione G., Gualandris A., 2018, MNRAS, 475, 4986

Fragione G., Loeb A., 2017, MNRAS, 55, 32

Frank J., Rees M. J., 1976, MNRAS, 176, 633

Gnedin O. Y., Gould A., Miralda-Escudé J., Zentner A. R., 2005, ApJ, 634, 344

Gualandris A., Portegies Zwart S., 2007, MNRAS, 376, L29

Gualandris A., Portegies Zwart S., Sipior M. S., 2005, MNRAS, 363, 223

Guillochon J., Loeb A., 2015, ApJ, 806, 124

Guillochon J., Ramirez-Ruiz E., 2013, ApJ, 767, 25

Gültekin K. et al., 2009, ApJ, 698, 198

Heacox W. D., 1998, AJ, 115, 325

Hills J. G., 1988, Nature, 331, 687

Hills J. G., 1989, BAAS, 21, 796

Kenyon S. J., Bromley B. C., Brown W. R., Geller M. J., 2014, ApJ, 793, 122

Kenyon S. J., Bromley B. C., Geller M. J., Brown W. R., 2008, ApJ, 680, 312

Kobulnicky H. A., Fryer C. L., 2007, ApJ, 670, 747

Kollmeier J. A., Gould A., 2007, ApJ, 664, 343

Levin Y., 2006, ApJ, 653, 1203

Lightman A. P., Shapiro S. L., 1977, ApJ, 211, 244

Lodato G., King A. R., Pringle J. E., 2009, MNRAS, 392, 332

LSST Science Collaboration et al., 2009, preprint (arXiv:0912.0201)

Lu Y., Yu Q., Lin D. N. C., 2007, ApJ, 666, L89

Löckmann U., Baumgardt H., 2008, MNRAS, 384, 323

Magorrian J., Tremaine S., 1999, MNRAS, 309, 447

Mainetti D., Lupi A., Campana S., Colpi M., Coughlin E. R., Guillochon J., Ramirez-Ruiz E., 2017, A&A, 600, A124

Mandel I., Levin Y., 2015, ApJ, 805, L4

Marchetti T., Contigiani O., Rossi E. M., Albert J. G., Brown A. G. A., Sesana A., 2018b, MNRAS, 476, 4697

Marchetti T., Rossi E. M., Brown A. G. A., 2018a, MNRAS

Miralda-Escudé J., Gould A., 2000, ApJ, 545, 847

O'Leary R. M., Loeb A., 2008, MNRAS, 383, 86

Perets H. B., 2009, ApJ, 698, 1330

Peters P. C., 1964, Phys. Rev., 136, 1224

Quinlan G. D., 1996, New A, 1, 35

Rein H., Liu S.-F., 2012, A&A, 537, A128

Rein H., Spiegel D. S., 2015, MNRAS, 446, 1424

Rossi E. M., Kobayashi S., Sari R., 2014, ApJ, 795, 125

Rossi E. M., Marchetti T., Cacciato M., Kuiack M., Sari R., 2017, MNRAS,

Sesana A., Haardt F., Madau P., 2006, ApJ, 651, 392

Sesana A., Haardt F., Madau P., 2007a, MNRAS, 379, L45

Sesana A., Haardt F., Madau P., 2007b, ApJ, 660, 546

Sesana A., Haardt F., Madau P., 2008, ApJ, 686, 432

Sesana A., Madau P., Haardt F., 2009, MNRAS, 392, L31

Sherwin B. D., Loeb A., O'Leary R. M., 2008, MNRAS, 386, 1179

Stone N. C., Metzger B. D., 2016, MNRAS, 455, 859

Wang J., Merritt D., 2004, ApJ, 600, 149 Wang Y.-H., Leigh N., Yuan Y.-F., Perna R., 2018, MNRAS, 475, 4595 Yu Q., 2002, MNRAS, 331, 935 Yu Q., Tremaine S., 2003, ApJ, 599, 1129 Zier C., Biermann P. L., 2001, A&A, 377, 23

APPENDIX A: ADDITIONAL FIGURES

In this appendix, we expand some of the figures presented in the paper to our full parameter space.

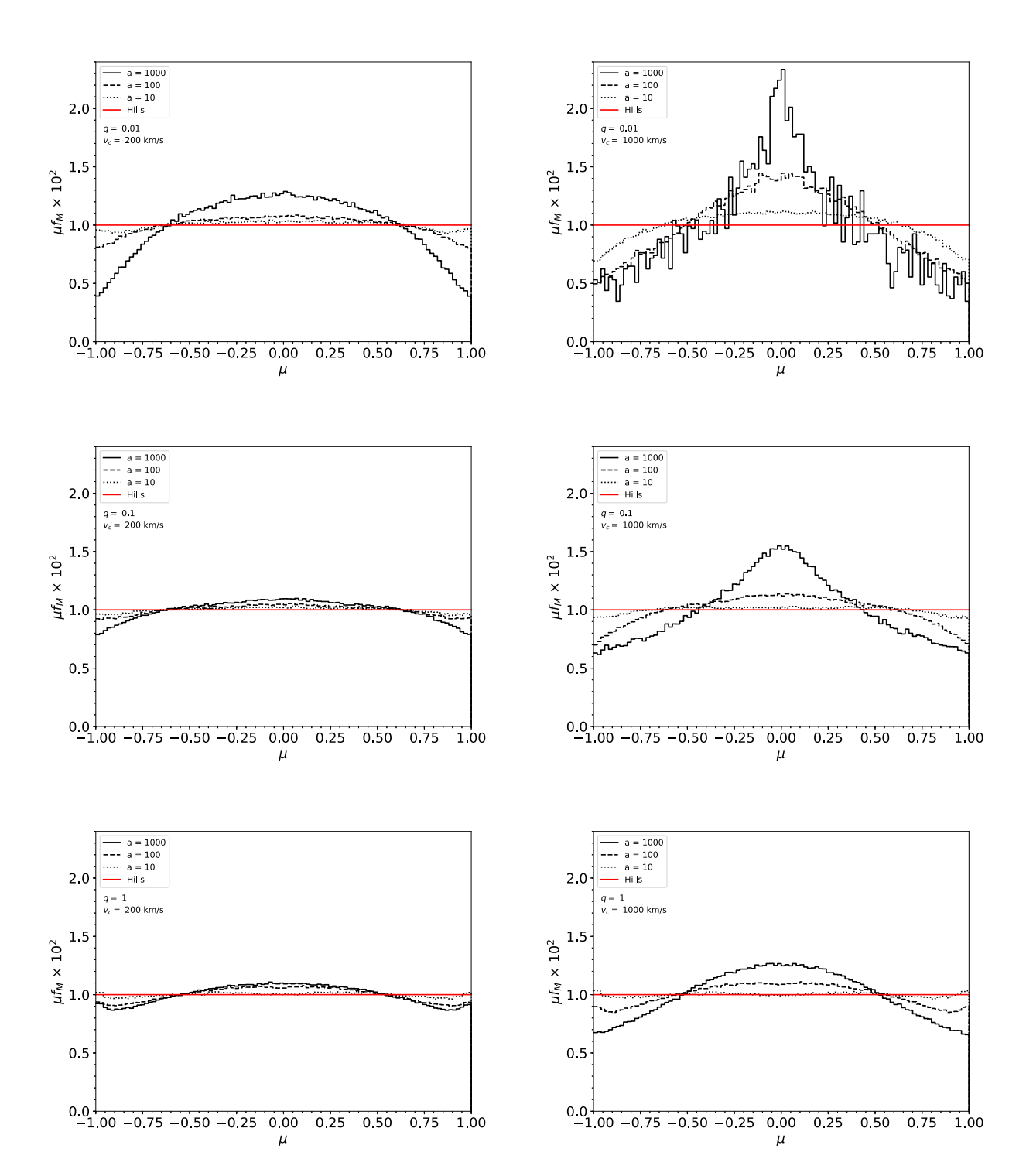


Figure A1. The probabilities μf_M for the direction cosine $\mu = \cos \theta = v_{z,\infty}/v_\infty$ of ejected stars at $\tilde{r}/\tilde{a} \to \infty$ for different binary SMBH mass ratios q and velocity cut-offs $\tilde{V} > v_c$. The PDF is $f_M \equiv f_M(\mu)$. The variable θ is the polar angle measured from the direction normal to the binary SMBH orbital plane. The top panels show the results for q = 0.01, the centre ones for q = 0.1, and the bottom ones for q = 1. The left-hand panels show ejections with $v_c = 200 \, \mathrm{km \, s^{-1}}$ and the right ones show those with $v_c = 1000 \, \mathrm{km \, s^{-1}}$. The linear bin widths are $\Delta_{\mu} = 0.02$. The red curve shows the uniform distribution for μ produced by the Hills mechanism.

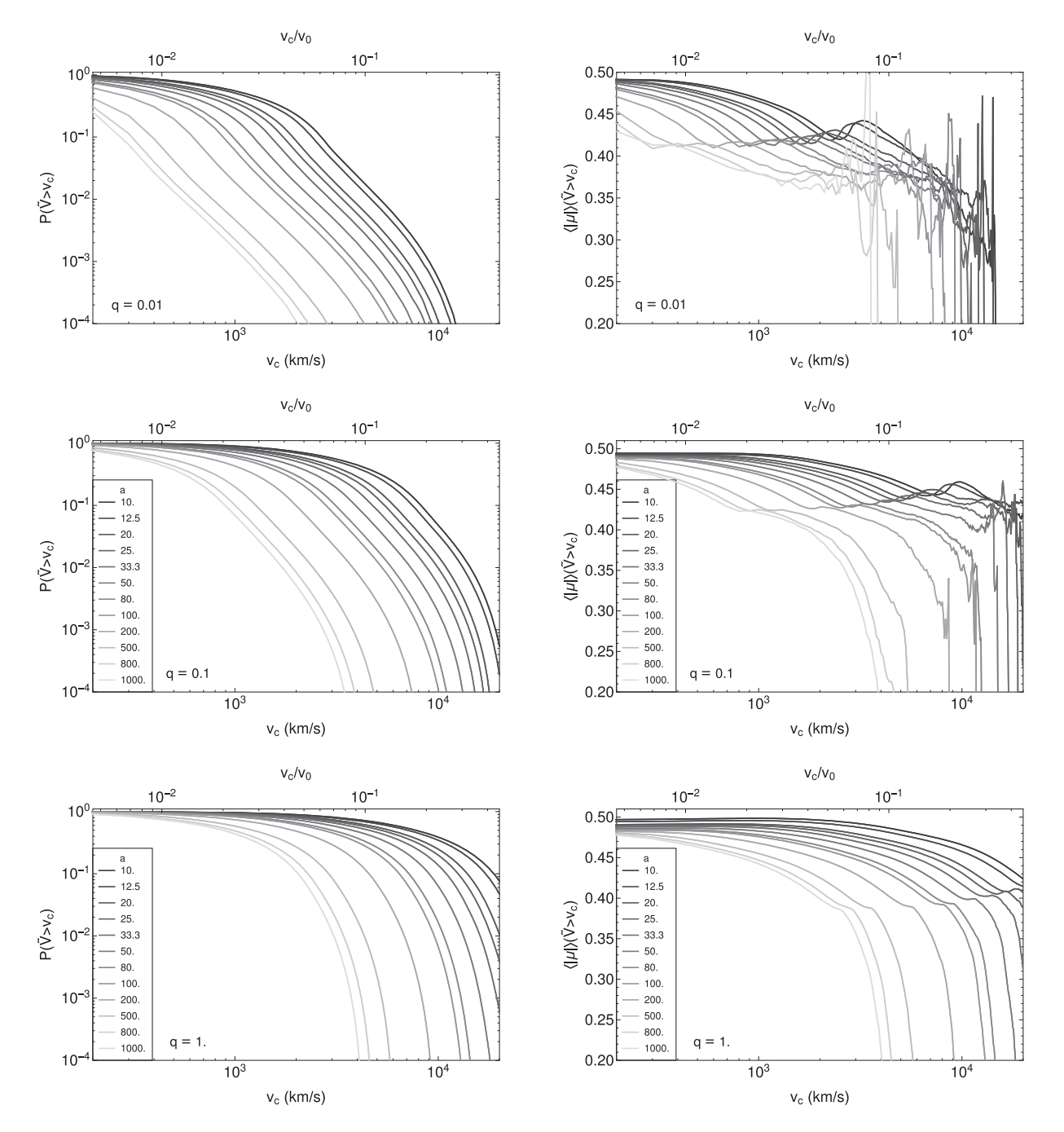


Figure A2. Statistics of ejected stars with a range of velocity cut-offs $\tilde{V} > v_c$. The top panels show the results for q = 0.01, the centre ones for q = 0.1, and the bottom ones for q = 1. The left-hand panels show the probability $P(\tilde{V} > v_c)$ that an ejected star has a velocity $\tilde{v}_{\infty} > v_c$. The right-hand panels show the orientation of ejected stars with velocities $v_{\infty} > v_c$; the orientation is parametrized by $\mu = \cos\theta = v_{z,\infty}/v_{\infty}$, where θ is the polar angle measured from the direction normal to the binary SMBH orbital plane. For an isotropic distribution, $\langle |\mu| \rangle = 0.5$.

This paper has been typeset from a TEX/IATEX file prepared by the author.